

Effects of Wake Turbulence on Aircraft Wing Section Numerical Study

by

Nur Hazwany Bt Mohd Hatta

Dissertation submitted in partial fulfillment of
the requirements for the
Bachelor of Engineering (Hons)
(Mechanical Engineering)

JANUARY 2009

Universiti Teknologi PETRONAS
Bandar Seri Iskandar
31750 Tronoh
Perak Darul Ridzuan

CERTIFICATION OF APPROVAL

Effects of Wake Turbulence on Aircraft Wing Section Numerical Study

by

Nur Hazwany Bt Mohd Hatta

A project dissertation submitted to the
Mechanical Engineering Programme
Universiti Teknologi PETRONAS
in partial fulfillment of the requirement for the
BACHELOR OF ENGINEERING (Hons)
(MECHANICAL ENGINEERING)

Approved by,

(Dr. Ahmed Maher Said Ali)

UNIVERSITI TEKNOLOGI PETRONAS

TRONOH, PERAK

January 2009

CERTIFICATION OF ORIGINALITY

This is to certify that I am responsible for the work submitted in this project, that the original work is my own except as specified in the references and acknowledgements, and that the original work contained herein have not been undertaken or done by unspecified sources or persons.

NUR HAZWANY BT MOHD HATTA

ABSTRACT

Fundamental of wake turbulence effects on aircraft wing section is determined by using numerical approach. NACA 2412 wing section is selected in this study and the wing is model using GAMBIT 2.2 software. For the numerical analysis, the flow past over the wing was simulated using computational fluid dynamics (CFD) software FLUENT 6.2. Simulations were carried out at different velocities at low Reynolds number and different angle of attack, α . The fundamental aerodynamic of wake effects analyzed from lift and drag coefficient values obtained from simulations that have been carried out. The outcome shows that the wake turbulence affected the lift and drag force of preceding aircraft is subjected to separation distance.

ACKNOWLEDGEMENT

I would like to take this opportunity to offer my sincerest acknowledgements to everyone that involves and helping me through this study. Firstly, my family for all the encouragement and advice they have given me to focus on this project. Next is my supervisor Dr Ahmed Maher Said Ali for guiding me through this study, helping me overcomes difficulties encountered and valuable suggestions throughout the study. A special thanks to Mr Timothy Ganesan for helping me in understanding the CFD software FLUENT 6.2 and result analysis using the software. Last but not least, to Mechanical Engineering Department lecturers and staff that gives good comments on this study during seminar and cooperation of using the computer lab to complete the simulations.

TABLE OF CONTENTS

CERTIFICATION OF APPROVAL	i
CERTIFICATION OF ORIGINALITY	ii
ABSTRACT	iii
ACKNOWLEDGEMENT	iv
LIST OF FIGURES	vi
LIST OF TABLES	viii
CHAPTER 1 INTRODUCTION	1
1.1 Background of the Study.....	1
1.2 Problem Statement	2
1.3 Objectives and Scope of Study	2
1.4 The Relevancy of Project.....	3
1.5 Feasibility of Project	3
CHAPTER 2 LITERATURE REVIEW	4
2.1 Wake Formation.....	4
2.2 Governing Equations and Numerical Method.....	5
CHAPTER 3 METHODOLOGY	7
CHAPTER 4 RESULTS AND DISCUSSION	8
4.1 Modelling	8
4.2 Simulations.....	12
4.3 Discussions.....	18
4.4 Comparison with Experiment Results.....	25
CHAPTER 5 CONCLUSIONS AND RECOMMENDATIONS	37
5.1 Conclusions	37
5.2 Recommendations	38
REFERENCES	39
LIST OF APPENDIX	40

LIST OF FIGURES

Figure 2.1: Wake formation	4
Figure 4.1: Mesh for single airfoil model	9
Figure 4.2: Outlet view of single airfoil model mesh	10
Figure 4.3: Mesh elements for single airfoil model at 6° AoA	10
Figure 4.5: Mesh for two airfoils model separated at one chord length at 4° AoA	11
Figure 4.4: Mesh element for two airfoils model at two chord lengths separation distance and 16° AoA	11
Figure 4.6: Boundary condition specification	13
Figure 4.7: Velocity inlet boundary condition window	13
Figure 4.8: Initialisation window	14
Figure 4.9: Residual monitors window	15
Figure 4.10: Iteration window	15
Figure 4.11: Reference value window	16
Figure 4.12: Force report	17
Figure 4.13: Lift coefficient versus angle of attack for single airfoil, 2 airfoils at 0.13 m separation distance and 2 airfoils at 0.26 m separation distance	20
Figure 4.14: Drag coefficient versus angle of attack for single airfoil, 2 airfoils at 0.13 m separation distance and 2 airfoils at 0.26 m separation distance	20
Figure 4.15: Lift coefficient versus angle of attack for single airfoil, 2 airfoils at 0.13 m separation distance and 2 airfoils at 0.26 m separation distance	21
Figure 4.16: Drag coefficient versus angle of attack for single airfoil, 2 airfoils at 0.13 m separation distance and 2 airfoils at 0.26 m separation distance	21
Figure 4.17: Lift coefficient versus angle of attack for single airfoil, 2 airfoils at 0.13 m separation distance and 2 airfoils at 0.26 m separation distance	22
Figure 4.18: Drag coefficient versus angle of attack for single airfoil, 2 airfoils at 0.13 m separation distance and 2 airfoils at 0.26 m separation distance	22
Figure 4.19: Velocity vectors for single airfoil at 0° AoA at 30 m/s	23
Figure 4.20: Velocity vectors for two airfoils separated at one chord length, 0.13 m at 0° AoA at 30 m/s	23
Figure 4.21: Velocity vectors for two airfoils separated at 2 chord length 0.26 m 0° AoA at 30 m/s	24
Figure 4.22: Comparison of numerical and experimental results of lift coefficient versus angle of attack for single airfoil	28
Figure 4.23: Comparison of numerical and experimental results of drag coefficient versus angle of attack for single airfoil	28
Figure 4.24: Comparison of numerical and experimental results of lift coefficient versus angle of attack for single airfoil	29

Figure 4.25: Comparison of numerical and experimental results of drag coefficient versus angle of attack for single airfoil	29
Figure 4.26: Comparison of numerical and experimental results of lift coefficient versus angle of attack for single airfoil	30
Figure 4.27: Comparison of numerical and experimental results of drag coefficient versus angle of attack for single airfoil	30
Figure 4.28: Comparison of numerical and experimental results of lift coefficient versus angle of attack for two airfoil at 0.13 m separation distance	31
Figure 4.29: Comparison of numerical and experimental results of drag coefficient versus angle of attack for two airfoil at 0.13 m separation distance	31
Figure 4.30: Comparison of numerical and experimental results of lift coefficient versus angle of attack for two airfoil at 0.13 m separation distance	32
Figure 4.31: Comparison of numerical and experimental results of drag coefficient versus angle of attack for two airfoil at 0.13 m separation distance	32
Figure 4.32: Comparison of numerical and experimental results of lift coefficient versus angle of attack for two airfoil at 0.13 m separation distance	33
Figure 4.33: Comparison of numerical and experimental results of drag coefficient versus angle of attack for two airfoil at 0.13 m separation distance	33
Figure 4.34: Comparison of numerical and experimental results of lift coefficient versus angle of attack for two airfoil at 0.26 m separation distance	34
Figure 4.35: Comparison of numerical and experimental results of drag coefficient versus angle of attack for two airfoil at 0.26 m separation distance	34
Figure 4.36: Comparison of numerical and experimental results of lift coefficient versus angle of attack for two airfoil at 0.26 m separation distance	35
Figure 4.37: Comparison of numerical and experimental results of drag coefficient versus angle of attack for two airfoil at 0.26 m separation distance	35
Figure 4.38: Comparison of numerical and experimental results of lift coefficient versus angle of attack for two airfoil at 0.26 m separation distance	36
Figure 4.39: Comparison of numerical and experimental results of drag coefficient versus angle of attack for two airfoil at 0.26 m separation distance	36

LIST OF TABLES

Table 1.1: MTOM with respect to aircraft categories	3
Table 4.1: Boundary conditions for the model	9
Table 4.2: Turbulence model with respect to AoA and velocity	12
Table 4.3: Stall angle	18
Table 4.4: Simulations result	19
Table 4.5: Stall angle comparison	25

ABBREVIATIONS AND NOMENCLATURE

NACA	National Advisory Committee for Aeronautics
AoA	Angle of attack
C_L	Lift coefficient
C_D	Drag coefficient

CHAPTER 1

INTRODUCTION

The most dangerous phases of wake turbulence are during the take-off and landing. This is due to the limited height of recovery thus makes it impossible for an aircraft to counter the wake turbulence in those phases compared during the flight phase. In order to understand this phenomenon, it is significant to understand the fundamental formation of the wake turbulence and the effects to the aircraft. There are various components of wake turbulence. However, the most important components are jetwash and wing vortices. The jetwash is turbulence form by the aircraft engine. It is turbulence and move rapidly but only for short duration. Wing vortices however, is extremely turbulent form at the wing tip of wing section due to pressure differential and can last in the air up to three minutes. It makes up as the primary and the most important component of wake turbulence. In fixed-wing aircraft, the wake vortices begin to form as the nose rotates for take-off. The turbulence then continues producing until the nose-wheel touches down the runway again. Crossing behind or below the leading aircraft are problems which cause by the vortices. Wake turbulence separation is provided by Air Traffic Control (ATC) to avoid accident during take-off and landing phases. Besides ATC, it is also pilot's responsibility to provide adequate spacing from preceding, arriving or departing aircraft in order to avoid accident cause by wake turbulence.

1.1 Background of the Study

Many studies of the wake turbulence effects on aircraft have been done with various approaches either experimentally or numerically. However, for simplification the study focuses on the aircraft wing section only. This reason behind this is because the wing section is the part that generates the lift of an aircraft and it is the location of wake turbulence formation. Thus, by studying the effects of wake turbulence of on the wing section we can conclude that the effects to the whole aircraft are the same as well.

1.2 Problem Statement

1.2.1 Problem Identification

Wake turbulence produce rolling moment which trails behind an aircraft signify a potential hazard for the preceding aircraft. Certain separation distances required to be maintained behind the leading aircraft to avoid fatal accidents.

1.2.2 Significance of the Project

The significance of the project carried out using numerical analysis is to obtain accurate outcome. Besides, using numerical analysis of the flow field such as pressure contour, velocity vector, turbulence intensity and etc can be done where it cannot be achieved in experimental. In addition, numerical analysis can extend the study by varying any parameters to achieve the objectives without limitations. Numerical approach saves cost, energy and time compared to experiment as the work is done by using computer and software

1.3 Objectives and Scope of Study

The objectives of this project are listed as below:

1. To study the aerodynamics effects of the wake field on aircraft wing section numerically. The simulation carried study the drag and lift coefficients characteristics of single airfoil, two airfoils separated at one chord length (one separation distance) and two airfoils separated at two chord length (two separation distance) at various free stream velocity and angle of attack.
2. To validate the numerical results by comparing with experimental result. The importance of the validation is to ensure that the simulation results obtained from the three main cases mentioned above are reliable and can be used to extend the study on other separation distance.

1.4 The Relevancy of Project

NACA 2412 wing section has been identified as the highest Due to hazardous condition that wake turbulence can brings, International Civil Aviation Organization (ICAO) had come out with minimum separation based on Maximum Take-Off Mass (MTOM) of the aircraft (Refer Table 1.1).

Table 1.1: MTOM with respect to aircraft categories

Categories	MTOM (kg)
Light	≤ 7000
Medium	$7000 < x < 136,000$
Heavy	≥ 136000

Each categories have it owns number of separation criteria for landing, take-off and en-route phases. The sequence of aircraft which making instrument approaches with regard to these minima will be controlled by Air Traffic Controller (ATC). For aircraft which making visual approach are advised of the relevant recommended spacing and are expected to maintain required separation.

1.5 Feasibility of Project

The project managed to complete within the time frame. However, literature works and simulations need to be done concurrently to ensure the smoothness of the project.

CHAPTER 2

LITERATURE REVIEW

2.1 Wake Formation

The shape of the airfoil makes the air move faster on the upper surface compared to the lower and thus creates pressure difference. Higher pressure on the lower surface generates lift force. The point where the air divides to flow on the airfoil known as stagnation point. As the angle of attack increases, the stagnation point moves rearward. As a result, the acceleration of air over the upper surface increases as well as the downward push on the air which increasing the total lift [1]. However, on the upper surface the air is also increasingly separates, increasing the drag and large amount of turbulent thus reduced the lift force. The angle where the lift force start to reduce known as the stall angle. The greater pressure under a wing forces the air outwards from the lower part of the wing, results in rotational flow at the tip vortex.

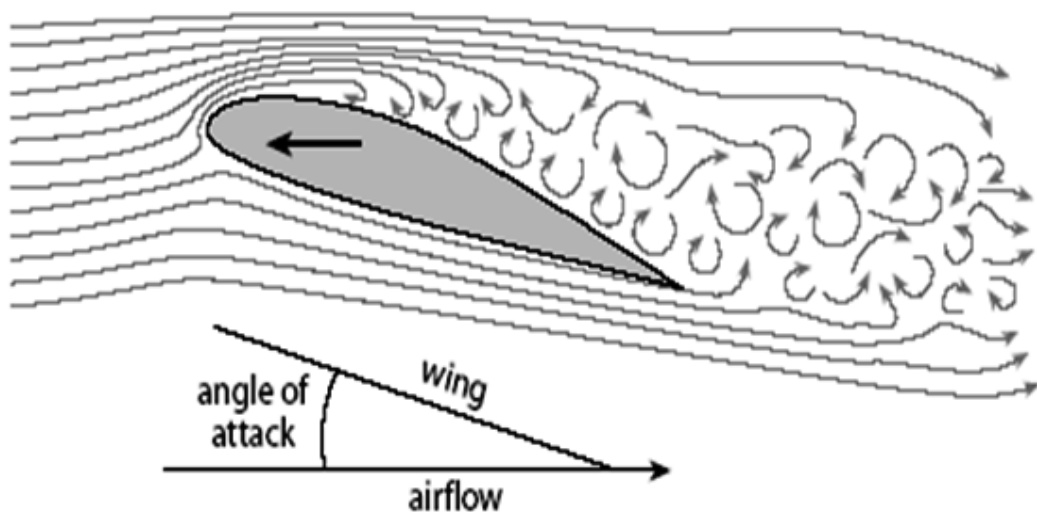


Figure 2.1: Wake formation [1]

2.2 Governing Equations and Numerical Method

The governing equations solved to analyze the turbulence property is the Navier-Stokes equation consists of a time-dependent continuity equation for conservation of mass, three time-dependent conservation of momentum equations x, y, and z direction. K-ε turbulence model focuses on the mechanisms that affect the turbulent kinetic energy. There are three types of k-ε turbulence model used which are standard k-ε model, RNG k-ε model and Realizable k-ε model.

Continuity equation:

$$\frac{\delta \rho}{\delta t} + \frac{\delta}{\delta x_i} (\rho u_i) = 0$$

Reynolds-averaged Navier-Stokes (RANS) are given by:

$$\frac{\delta}{\delta t} (\rho u_i) + \frac{\delta}{\delta x_j} (\rho u_i u_j) = -\frac{\delta P}{\delta x_i} + \frac{\delta}{\delta x_j} \left[\mu \left(\frac{\delta u_j}{\delta x_j} + \frac{\delta u_i}{\delta x_i} - \frac{2}{3} \right) \sigma_{ij} \frac{\delta u_l}{\delta x_l} \right] + \frac{\delta}{\delta x_j} (-\rho \overline{u'_i u'_j})$$

Where the term $(-\rho \overline{u'_i u'_j})$ is numerically modeled to close the equation. All the simulations carried assumed the air is incompressible with density, ρ and viscosity, μ values 1.18 kg/m³ and 1.789 kg/m-s respectively.

2.2.1 Standard k – ε Model:

This is the frequently used model in general-purpose CFD codes. It is also the model used for the purposes of these particular simulations. This model was used for lower free stream velocities, i.e. u = 5m/s. The following are transport equations for turbulent kinetic energy (k) and its dissipation rate (ε):

$$\frac{\delta}{\delta t} (\rho k) + \frac{\delta}{\delta x_i} (\rho k u_i) = \frac{\delta}{\delta x_j} \left[\left(\mu + \frac{\mu_t}{\sigma_k} \right) \frac{\delta k}{\delta x_j} \right] + G_k + G_b - \rho \varepsilon - Y_m + S_k$$

$$\frac{\delta}{\delta t} (\rho \varepsilon) + \frac{\delta}{\delta x_i} (\rho \varepsilon u_i) = \frac{\delta}{\delta x_j} \left[\left(\mu + \frac{\mu_t}{\sigma_\varepsilon} \right) \frac{\delta \varepsilon}{\delta x_j} \right] + C_{1\varepsilon} \frac{\varepsilon}{k} (G_k + G_{3\varepsilon} G_b) + C_{2\varepsilon} \rho \frac{\varepsilon^2}{k} + S_\varepsilon$$

Based on the work by Sangupta and Sakar [2], the following constants are used:

$$C_{1\varepsilon} = 1.44, C_{2\varepsilon} = 1.92, \sigma_k = 1.00$$

2.2.2 RNG $k - \varepsilon$ Model:

RNG model (renormalization group theory) is an extension of the standard k -epsilon model. The RNG model includes an R term on the ε equation, this term depends on the rate of strain, given by:

$$R = \frac{\rho C_\mu \eta^3 \left(1 - \left(\frac{\eta}{\eta_0}\right)\right)}{(1 + \beta \eta^3)} \left(\frac{\varepsilon^2}{k}\right)$$

Where $\eta = Sk/\varepsilon$.

The default constants are given by: $C_{1\varepsilon} = 1.42, C_{2\varepsilon} = 1.68, C_\mu = 0.0845, \sigma_k = 1.0, \sigma_\varepsilon = 1.3, \eta_0 = 4.38$ and $b = 0.012$ [3]. This turbulence model has a higher computational cost than the standard model but more suitable for intermediate free stream velocities, i.e. $u = 30$ m/s

2.2.3 Realizable $k - \varepsilon$ Model

Transport equations are given by:

$$\frac{\delta}{\delta t}(\rho k) + \frac{\delta}{\delta x_i}(\rho k u_i) = \frac{\delta}{\delta x_i} \left[\left(\mu + \frac{\mu_t}{\sigma_k} \right) \frac{\delta k}{\delta x_j} \right] + G_k + G_b - \rho \varepsilon - Y_m$$

$$\frac{\delta}{\delta t}(\rho \varepsilon) + \frac{\delta}{\delta x_j} = \frac{\delta}{\delta x_j} \left[\left(\mu + \frac{\mu_t}{\sigma_\varepsilon} \right) \frac{\delta \varepsilon}{\delta x_j} \right] + \rho C_1 S_\varepsilon - \rho C_2 \frac{\varepsilon^2}{k + \sqrt{\nu \varepsilon}} + C_{1\varepsilon} \frac{\varepsilon}{k} C_{3\varepsilon} G_b + S_\varepsilon$$

Where $C_1 = \max \left[0.43, \frac{\eta}{\eta + 5} \right]$ and $\eta = S \frac{k}{\varepsilon}$

The realizable k -epsilon model produced reliable results for higher angle of attack and free stream velocities (i.e. $u > 30$ m/s).

CHAPTER 3

METHODOLOGY

GAMBIT 2.2 and FLUENT 6.2 are both commercial software chosen to study the effects of wake turbulence by running the simulations as both of the software are available in UTP Mechanical Computer Lab. In this study, the lift and drag coefficients of NACA 2412 airfoil at 10, 20 and 30 m/s at eleventh angle of attack start with 0° AoA until 20° AoA with 2° increment studied. NACA 2412 airfoil has been selected as this type of airfoil used widely in private aircraft and has been reported involved in several accidents [4]. Besides, the results obtained by numerical have to be validated with experiment which used NACA 2412 airfoil. There are three main simulations which are simulation of single airfoil, two airfoils separated at one chord length and two airfoils separated at two chord lengths. The wind tunnel test section dimension is 0.6 X 0.3 X 0.3 (m) and the chord length of the airfoil is 0.13 m following from the experiment. The single airfoil simulation was done to study the effects of wake turbulence on stall angle for single airfoil. The first simulation acted as base to compared and study the effects of wake turbulence occur in the second and third simulation stall angle. In the second case, the one chord length separation distance selected due to the limitation of wind tunnel test section for experiment. The maximum separation distance for the test section is two chord lengths and thus, the third case used the maximum allowable separation distance.

CHAPTER 4

RESULTS AND DISCUSSION

4.1 Modelling

Gambit software used to model the airfoils in wind tunnel with various angles of attack. Below are the steps taken in modelling process using Gambit software (Refer Appendix II for the figures).

- i. NACA 2412 airfoil coordinates using imported by *File-Import-ICEM Input*. After selected the filename, select vertices and edges. Deselect faces and Accept button clicked.
- ii. *Geometry Command Button* opened; select the *Face Command button* and *Form Face* button. All edges selected from edges list and close. *Apply* button clicked.
- iii. *Face Command* button closed, *Volume Command* button opened. Right-hand clicked at the *Form Volume* and *Sweep Face* selected. Under faces column, face that has been created before selected. By default, the name was *face.1*. Next, under path, *Vector-Define* selected. *Vector Definition* box popped-up and *Magnitude* selected. Specify the width of airfoil on *Magnitude* column and *Apply*.
- iv. *Volume Command* button closed. *Create Volume* opened. *Create Real Brick* box opened; specify the wind tunnel dimension and *Apply* clicked. Adjust the wind tunnel location using *Move/Copy/Align Volumes* button. For airfoil with certain angle of attack, specify the angle at *Rotate* column.
- v. Next, right-clicked on *Boolean Operations* and *Subtract* command selected. Under volume, wind tunnel volume selected and airfoil volume under subtract volume. Then *Apply*.
- vi. *Geometry Command* button closed and *Mesh Command* button opened. *Volume Command* button and *Mesh Volumes* selected. Volume created

selected under volumes column and elements changed to Tet/Hybrid and TGrid type. Under interval size spacing, 0.008 m specified and Apply. Mesh generated was not a uniform mesh and consists of tetrahedral, pyramids and prism elements (Refer Fig 4.1).

- vii. Mesh Command button closed, Zones Command button opened. Specify Boundary Types command selected and boundary conditions for the model specified then *Apply*.

Table 4.1: Boundary conditions for the model

Boundary Types	Faces	Remarks
Wall	Airfoil	face.1,face.2,face.3,face.4
Symmetry	Wind tunnel	face.5,face.6,face.9,face.10
Velocity_Inlet	Wind tunnel inlet	face.7
Outlet_Vent	Wind tunnel outlet	Face.8

- viii. Model exported. *File-Export-Mesh*. File name written as *NACA2412.msh* Ensure Export 2-D(X-Y) Mesh deselect and then *Accept*.

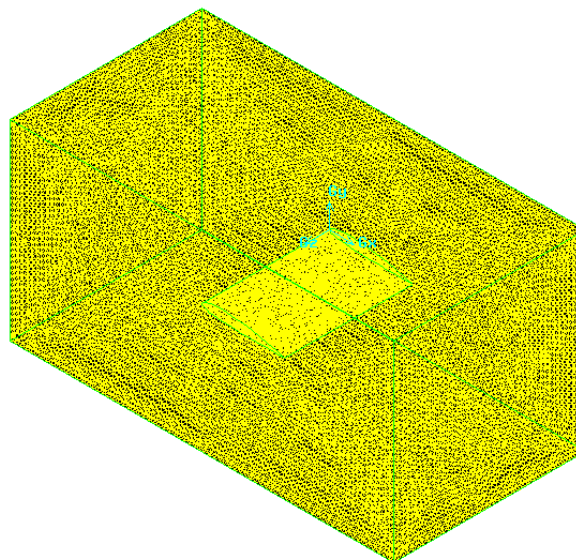


Figure 4.1: Mesh for single airfoil model

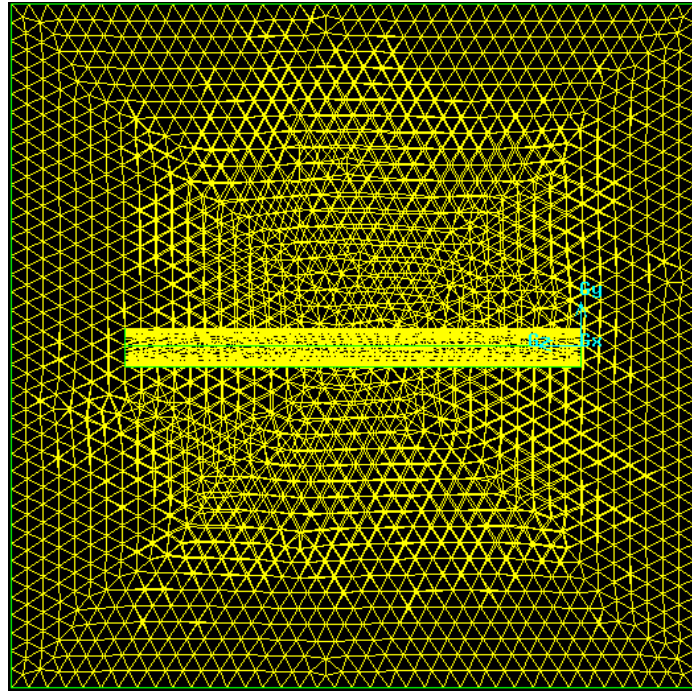


Figure 4.2: Outlet view of single airfoil model mesh

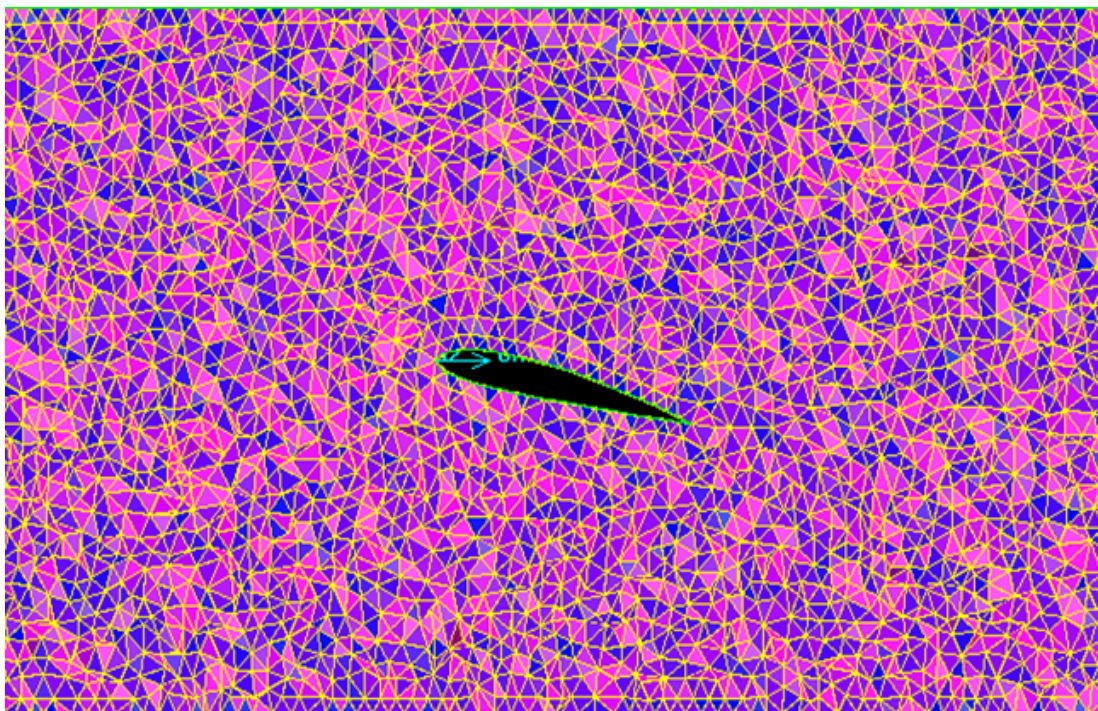


Figure 4.3: Mesh elements for single airfoil model at 6° AoA

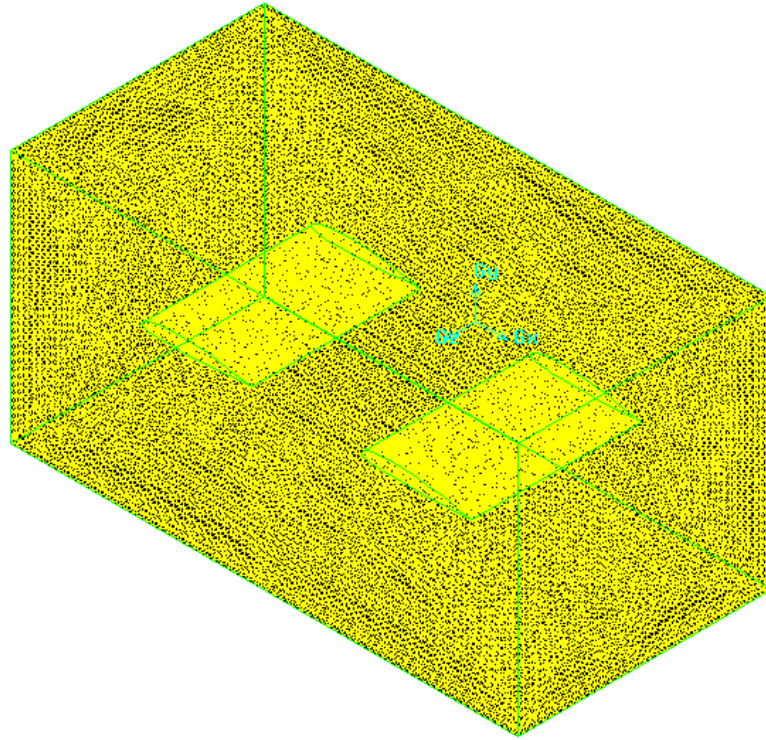


Figure 4.4: Mesh for two airfoils model separated at one chord length at 4° AoA

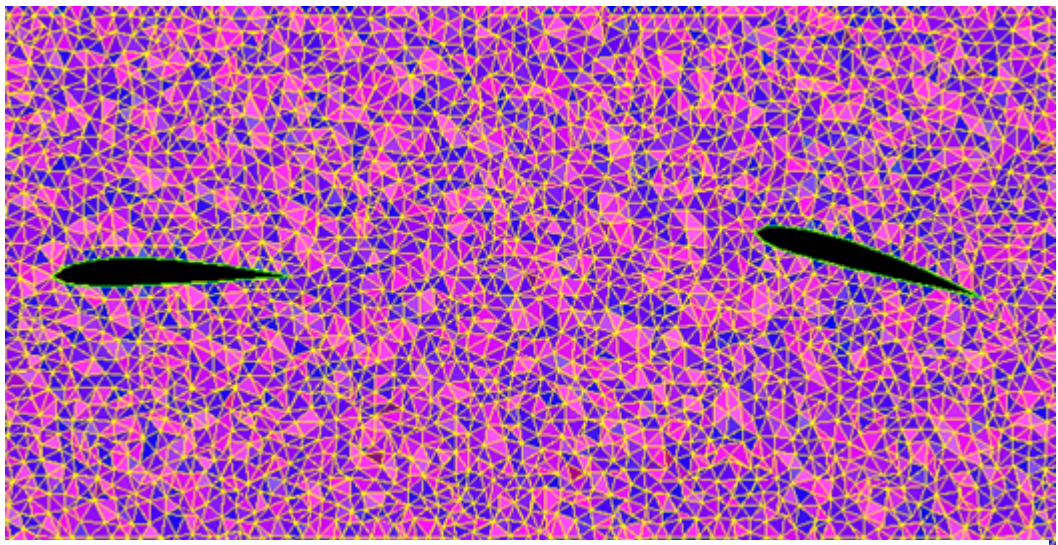


Figure 4.5: Mesh element for two airfoils model at two chord lengths separation distance and 16° AoA

4.2 Simulations

In each case, thirty-three simulations required- eleventh angle of attack ($0^\circ, 2^\circ, \dots, 18^\circ, 20^\circ$) and three velocities (10 m/s, 20 m/s and 30 m/s). Each of the simulation took at least seven hours to converge with 0.0001 convergence criterion and three hours with 0.001 convergence criterion. In this case, the convergence criterion used was 0.001 due to the time constraint. . The type of turbulence model used in each case depends on velocity and angle of attack (Refer Table 4.2).

Table 4.2: Turbulence model with respect to AoA and velocity

AoA	Velocity (m/s)	Turbulence Model	Discretization
0-14	10 & 20	Standard k- ϵ model, Standard Wall Functions	First order upwind
	30	RNG model, Enhanced Wall Treatment	First order upwind
16-22	10, 20 & 30	Realizable model, Enhanced Wall Treatment	Second order upwind

Following are the schemes of simulation settings in Fluent software:-

- i. Before Fluent window opened, Fluent version window opens. Left Click the 3ddp option and Left Click Run
- ii. Model/mesh NACA2412.msh just created in Gambit File-Read-Case opened. Locate the NACA2412.msh file just created in Gambit and Left Click Ok. The NACA2412.msh file read into Fluent, and when this is completed, Done appear at the bottom the window.
- iii. Next the grid created in Gambit checked for errors Grid-Check. If no errors occur the screen will look similar to the following after the grid check. The word Grid Check appear at the top of the screen, and the word Done appear at the bottom of the screen.
- iv. Define - Models -Viscous. Viscous Window appears and K-epsilon model selected. Next, refer table 4.1 for Viscous Model setting.
- v. Next the free stream velocity of the airflow around the wing needs set. In order to do select the following menus Define - Materials. The Materials window appears. On this screen the material properties of the substances in

the simulation, by default is air. Change the air density to 1.18 kg/m^3 . Left Click on Close.

- vi. Next the Boundary Conditions for the problem need to be defined. Select Define - Boundary Conditions. Left Click on Velocity_inlet and Left Click on Set. This caused the Velocity Inlet window to appear.

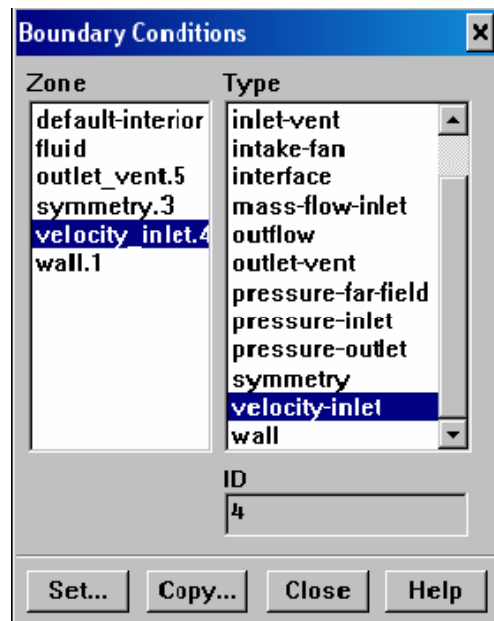


Figure 4.6: Boundary condition specification

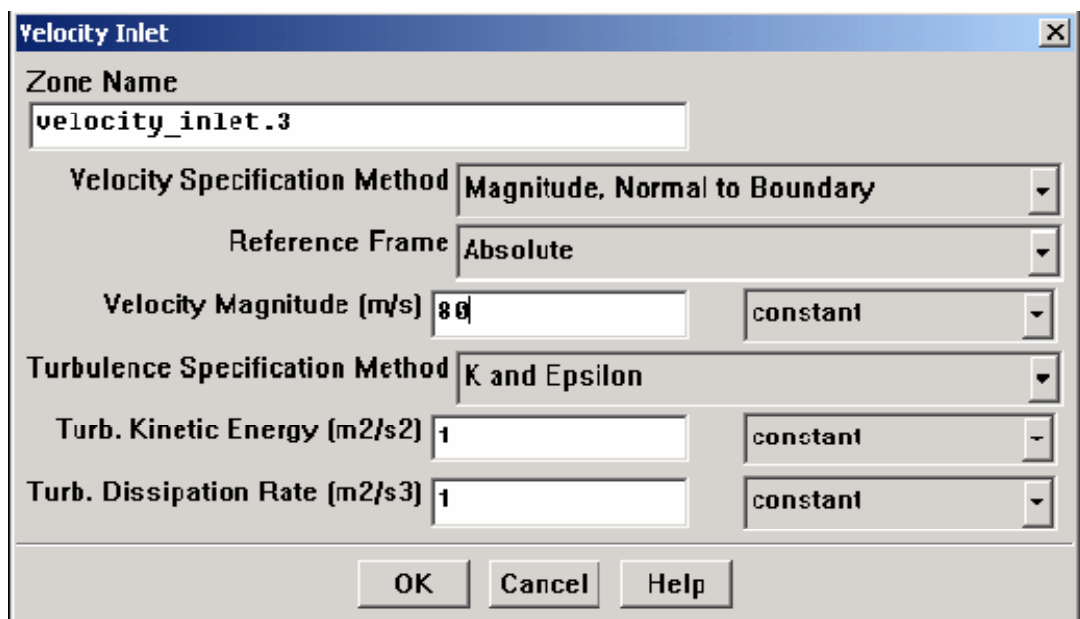


Figure 4.7: Velocity inlet boundary condition window

Enter the free stream velocity desired in the Velocity Magnitude (m/s) field. For the purposes of this simulation start with 10m/s and leave all other fields at their default settings. Left Click on OK. Left Click on Close on the Boundary Conditions window.

- vii. Next the numerical solution method for the simulation selected. To select the method complete the following. Solve Controls Solution Refer discretization scheme on Table 4.2.
- viii. Now the free stream velocity initialized. Solve - Initialize – Initialize. This opened the Solution Initialization window. Left Click the black downward arrow in the Compute From field. Select velocity_inlet.3. Left Click on Init. Left Click on Close.

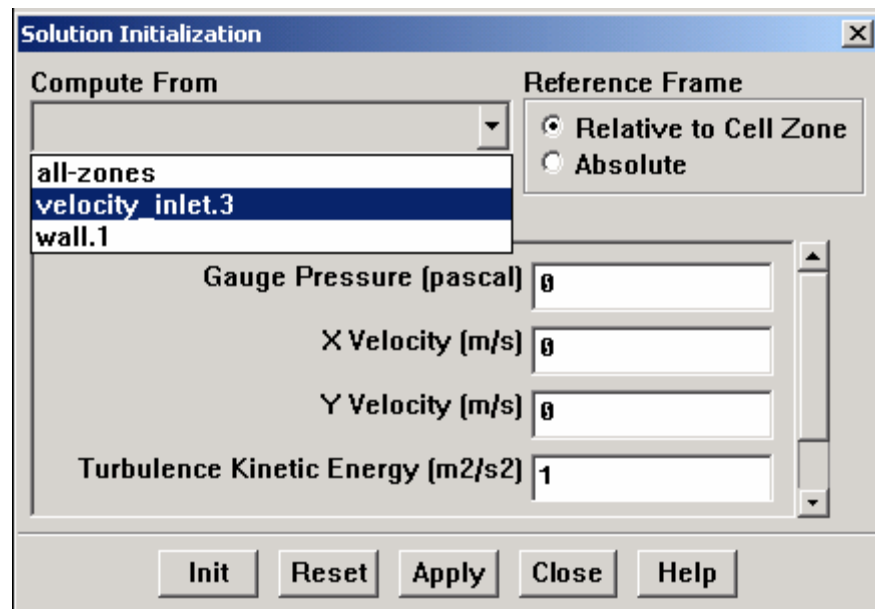


Figure 4.8: Initialisation window

- ix. Next the convergence parameters of the solution chosen. Solve - Monitors – Residual. This opened the Residual Monitors window. In the Options field make sure Print and Plot are selected. Change the Convergence Criterion for all residual monitors to 0.001 then close the Residual Monitors window

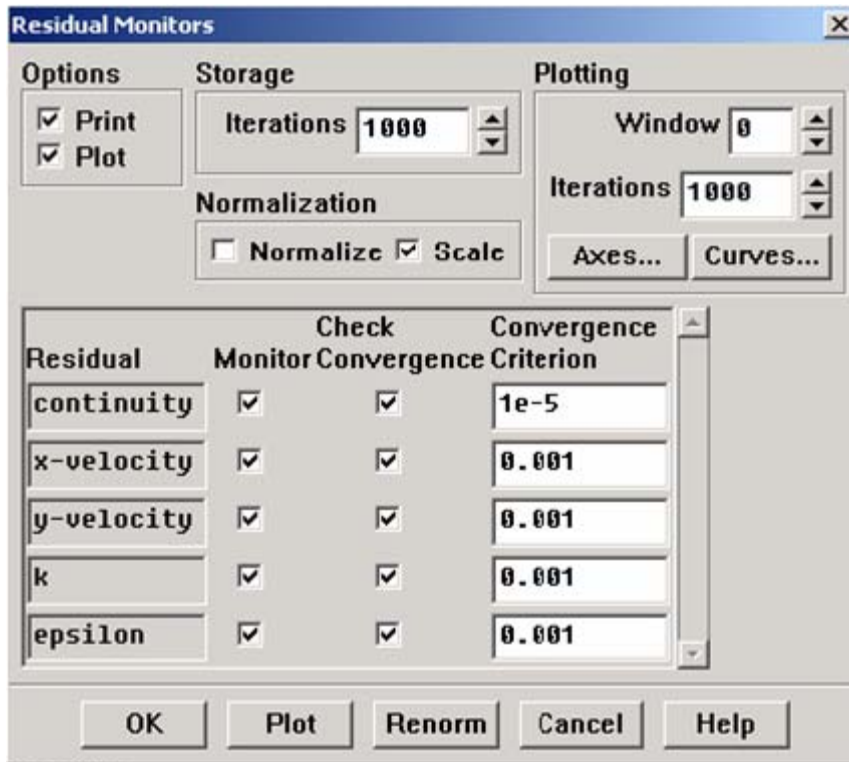


Figure 4.9: Residual monitors window

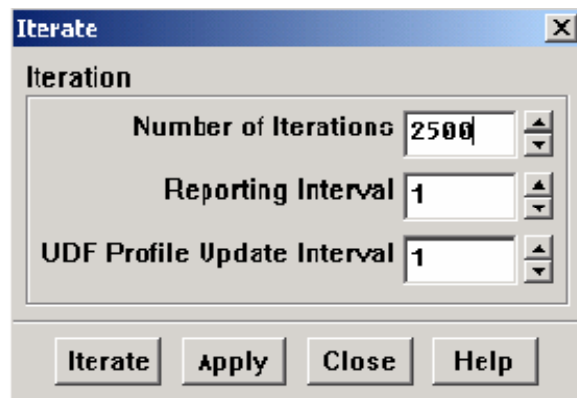


Figure 4.10: Iteration window

- x. Next the simulation can be started. Solve – Iterate. Change Number of Iterations to 1000. Left Click on Iterate
- xi. After the iteration converge, Report - Reference Values. The Reference Value window appears. The Reference Value window allows the entry of all the normalizing values into Fluent. In other words it will transform Lift and Drag forces into coefficients. For the purposes of this simulation the Velocity and Area (chord length) needs to be changed. First change the Velocity_field to 10 m/s. Next change the Area field to 0.026 m². Left Click on OK.

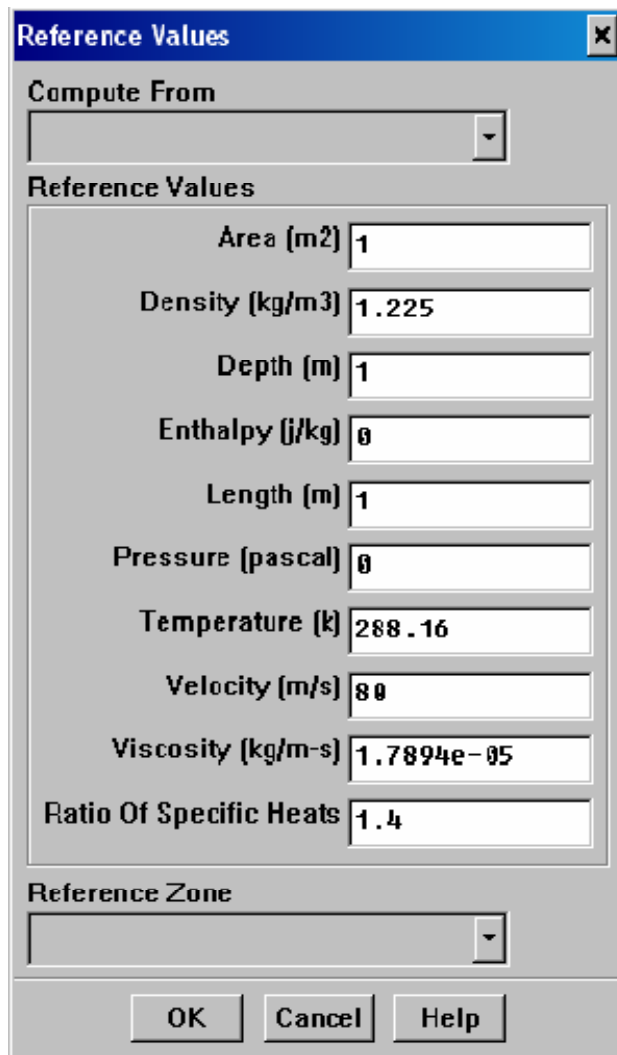


Figure 4.11: Reference value window

xii. Now that the forces have been normalized, Fluent is ready to report the correct coefficients. Display lift and drag coefficient start by selecting the following menus. Report - Forces. This opened the Force Reports window.

In order to display drag the following steps completed:-

- Under the Options field Left Click on Forces
- In the Force Vector field change X=1, Y=0
- Left Click on Print

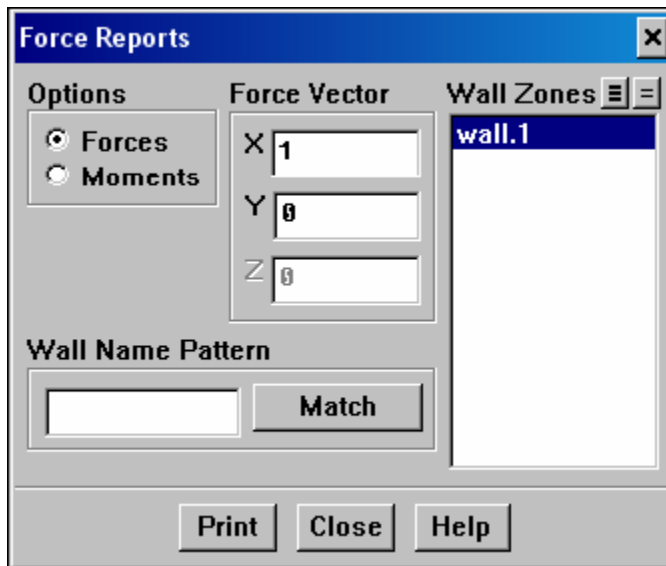


Figure 4.12: Force report

This caused the drag data to appear in Fluent's main window. Scroll the window all the way the right, and the final number displayed on the bottom row, labeled total coefficient, is the drag coefficient. Coefficient recorded.

To find lift, the Force Reports window opened. Forces were selected under the Options field. In the Force Vector field changed X=0, Y=1. Left Click on Print This caused the lift data to appear in Fluent's main window. Scroll the window all the way the right, and the final number displayed on the bottom row, labeled total coefficient, is the lift coefficient. Coefficient recorded.

4.3 Discussions

For all the three cases, the stall angle obtained shown in Table 4.3 below.

Table 4.3: Stall angle

No	Cases	Stall angle (°)
1	Single airfoil	18
2	Two airfoils with 0.13 m separation distance	14
3	Two airfoils with 0.26 m separation distance	20

For overall, the results (Refer Table 4.4) shows that the lift and drag coefficient value for the second case is smaller compared to the first and the third case (Refer Appendix III for each cases graphs). Besides, the lift coefficient value after the stall angle for the second case is increasing. In comparing with the first case, the smaller and instability of the value is due to the effects of wake turbulence from the front airfoil and the smaller separation distance which one chord length. Therefore, the air velocity received on preceding airfoil due to the turbulence was higher compared to the front airfoil and thus effects its lift and drag coefficient. Thus, lower the stall angle by half compared to the first case. For the third case, the separation distance between the two airfoil is significant and there are chances that the turbulence eddies demolish before arrive at the preceding airfoil. This explain why the value for lift and drag coefficient in the third case is higher compared to the second case but lower from the first case. By referring to the velocity vectors in Figure 4.19, Figure 4.20 and Figure 4.21, the velocity vectors for the three cases at zero angle of angle of attack with 30 m/s shows that the velocity reached the preceding airfoil in second case was higher indicated by the green colour as well as velocity surrounding the airfoil indicates by dark orange compared with the third case.

Table 4.4: Simulations result

Simulation 1 : Single airfoil						
AoA	Velocity (m/s)					
	10		20		30	
	C_L	C_D	C_L	C_D	C_L	C_D
0	0.105	0.085	0.104	0.066	0.111	0.048
2	0.221	0.090	0.209	0.072	0.187	0.069
4	0.326	0.102	0.311	0.083	0.313	0.063
6	0.437	0.118	0.416	0.097	0.417	0.076
8	0.551	0.141	0.526	0.118	0.528	0.095
10	0.666	0.168	0.636	0.143	0.636	0.118
12	0.780	0.203	0.745	0.176	0.743	0.149
14	0.893	0.242	0.854	0.215	0.848	0.185
16	1.033	0.297	0.969	0.258	0.925	0.205
18	1.052	0.284	1.011	0.256	0.989	0.244
20	1.035	0.320	0.972	0.287	0.925	0.269
Simulation 2 : Two airfoils at one chord length separation distance						
0	0.089	0.054	0.069	0.045	0.062	0.039
2	0.196	0.059	0.167	0.050	0.158	0.044
4	0.302	0.069	0.267	0.059	0.257	0.053
6	0.413	0.083	0.373	0.072	0.363	0.066
8	0.521	0.103	0.478	0.091	0.467	0.084
10	0.639	0.130	0.594	0.115	0.582	0.108
12	0.752	0.165	0.705	0.146	0.692	0.137
14	0.865	0.203	0.816	0.183	0.803	0.173
16	0.849	0.205	0.814	0.189	0.802	0.181
18	0.946	0.249	0.911	0.230	0.950	0.232
20	1.010	0.298	0.967	0.276	0.978	0.274
Simulation 3 : Two airfoils at two chord length separation distance						
0	0.095	0.057	0.078	0.047	0.071	0.041
2	0.195	0.062	0.172	0.052	0.165	0.046
4	0.299	0.071	0.271	0.060	0.265	0.055
6	0.408	0.086	0.377	0.074	0.372	0.068
8	0.515	0.105	0.485	0.091	0.481	0.085
10	0.626	0.131	0.595	0.115	0.591	0.108
12	0.736	0.164	0.707	0.145	0.702	0.137
14	0.742	0.162	0.723	0.149	0.723	0.146
16	0.829	0.200	0.815	0.186	0.815	0.183
18	0.908	0.209	0.891	0.266	0.830	0.223
20	1.115	0.326	1.056	0.298	1.021	0.284
22	1.067	0.348	1.021	0.334	0.997	0.318
24	1.024	0.45	1.01	0.42	0.989	0.392

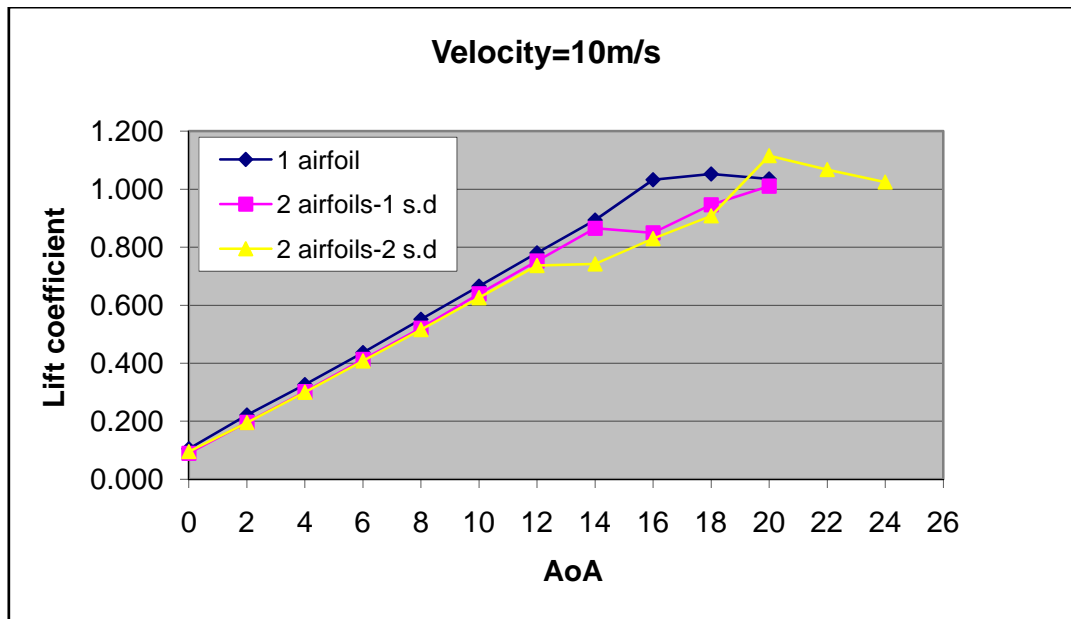


Figure 4.13: Lift coefficient versus angle of attack for single airfoil, 2 airfoils at 0.13 m separation distance and 2 airfoils at 0.26 m separation distance

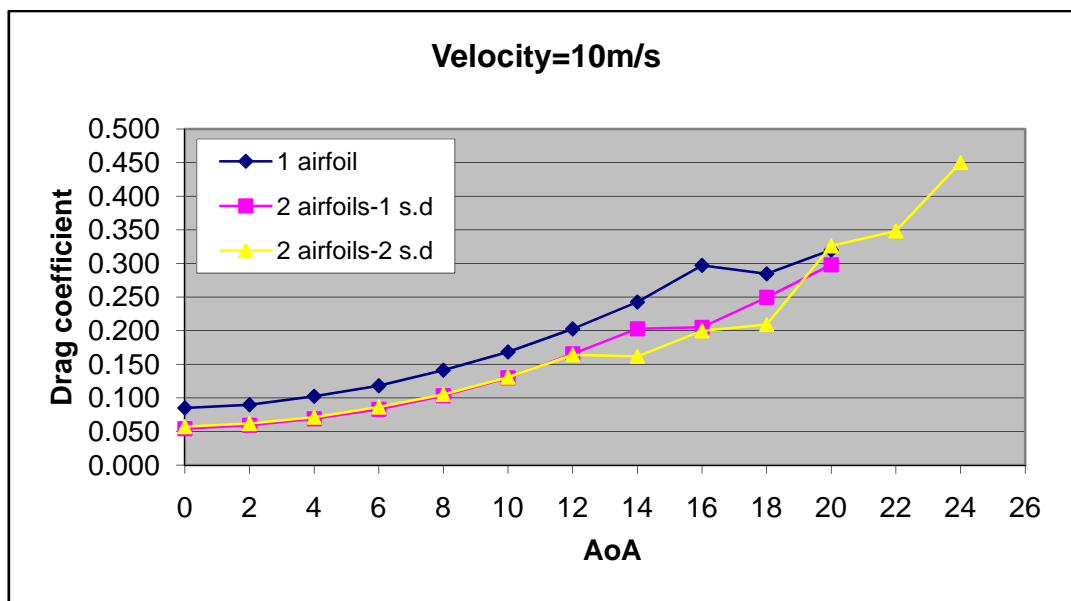


Figure 4.14: Drag coefficient versus angle of attack for single airfoil, 2 airfoils at 0.13 m separation distance and 2 airfoils at 0.26 m separation distance

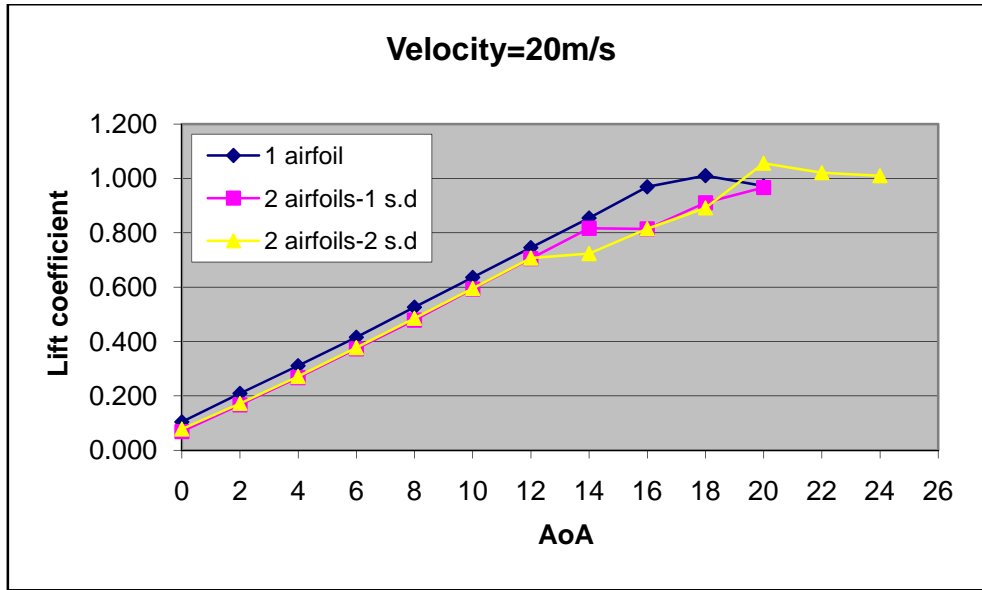


Figure 4.15: Lift coefficient versus angle of attack for single airfoil, 2 airfoils at 0.13 m separation distance and 2 airfoils at 0.26 m separation distance

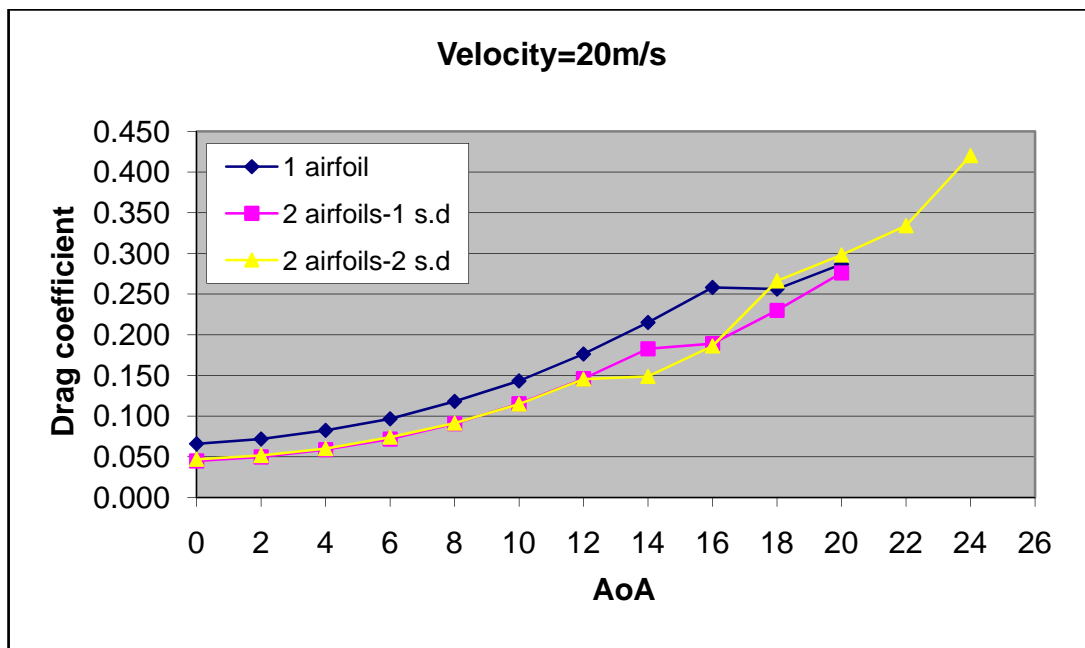


Figure 4.16: Drag coefficient versus angle of attack for single airfoil, 2 airfoils at 0.13 m separation distance and 2 airfoils at 0.26 m separation distance

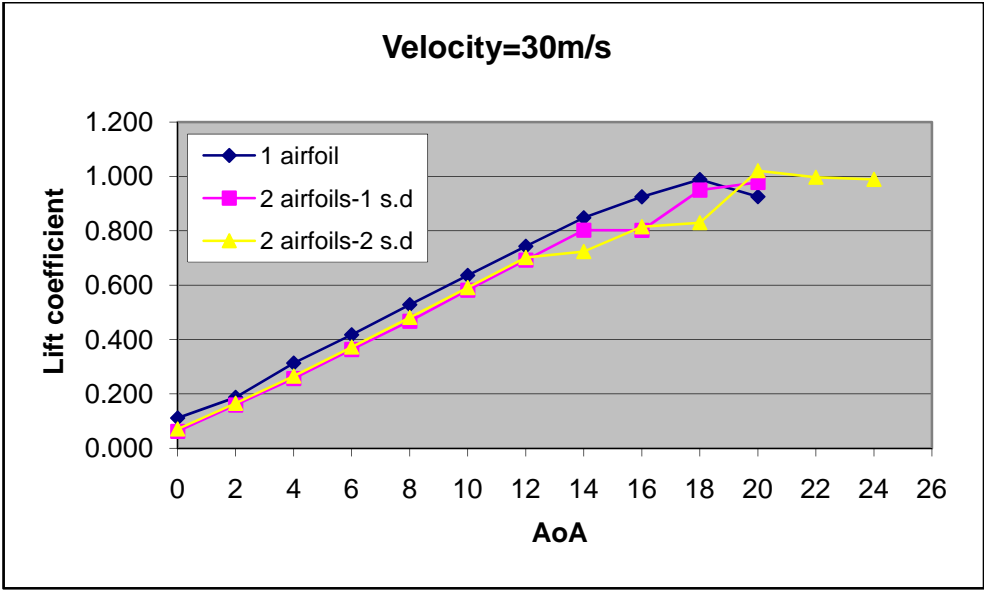


Figure 4.17: Lift coefficient versus angle of attack for single airfoil, 2 airfoils at 0.13 m separation distance and 2 airfoils at 0.26 m separation distance

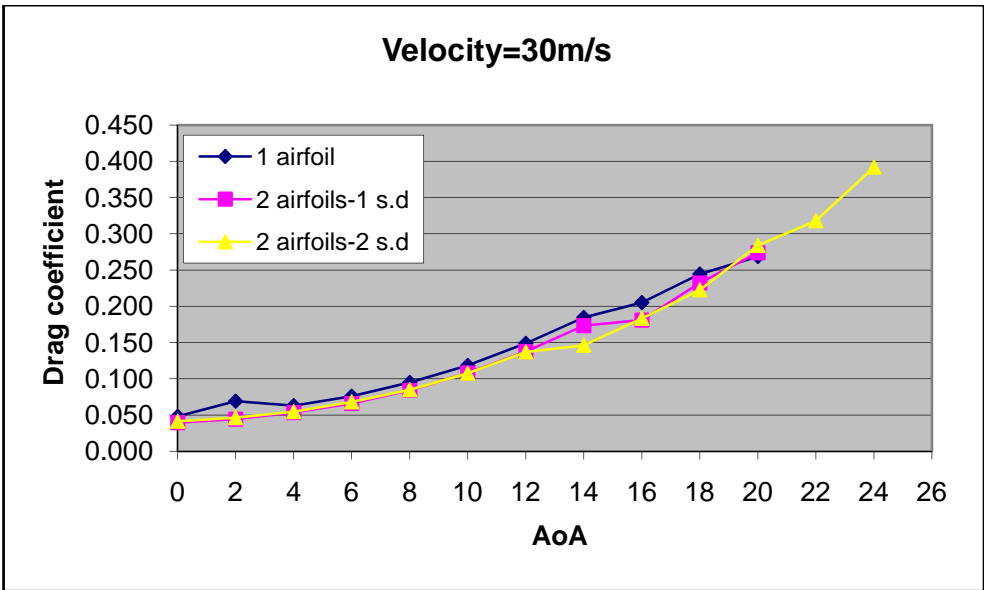


Figure 4.18: Drag coefficient versus angle of attack for single airfoil, 2 airfoils at 0.13 m separation distance and 2 airfoils at 0.26 m separation distance

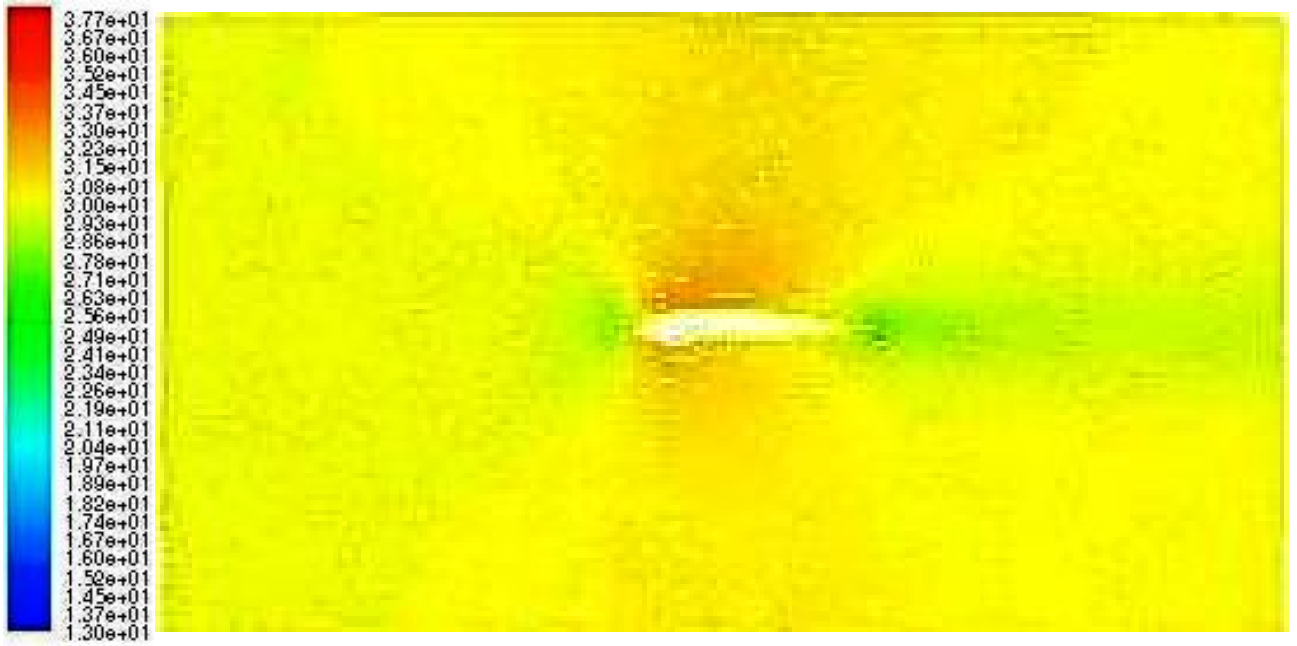
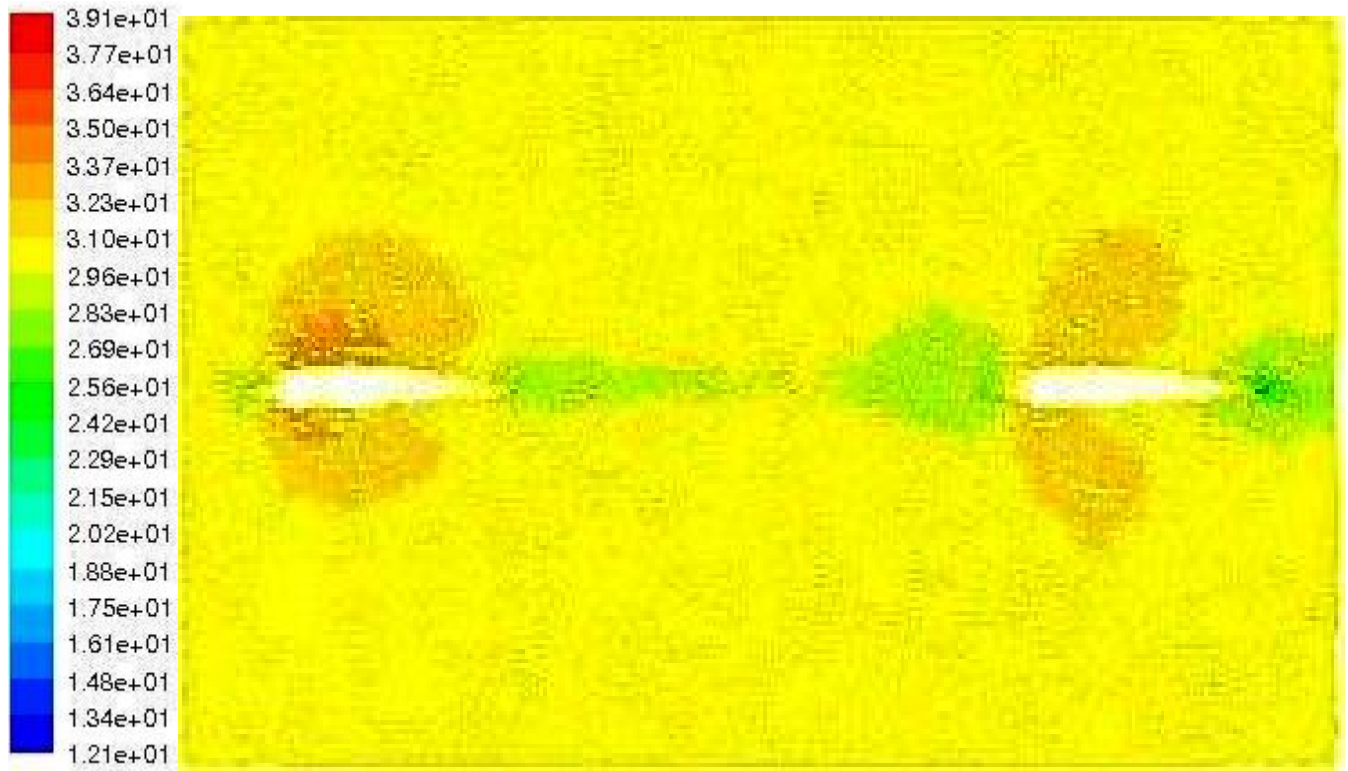


Figure 4.19: Velocity vectors for single airfoil at 0° AoA at 30 m/s



Figure 4.20: Velocity vectors for two airfoils separated at one chord length, 0.13 m at 0° AoA at 30 m/s



**Figure 4.21: Velocity vectors for two airfoils separated at 2 chord length 0.26 m
0° AoA at 30 m/s**

4.4 Comparison with Experiment Results

The value for lift and drag coefficient for all the case are approximate. However, there stall angle are difference between numerical and experiment as shown in Table 4.5 below.

Table 4.5: Stall angle comparison

No	Cases	Stall angle (°)	
		Numerical	Experiment
1	Single airfoil	18	16
2	Two airfoils with 0.13 m separation distance	14	18
3	Two airfoils with 0.26 m separation distance	20	16

4.4.1 Lift Coefficient

For lift coefficient, in each case, as the velocity increase the lift coefficient deviates.

However, for the first case at 10 m/s, the deviation trend approximated 22.4 percent from 0 to 8 degree AoA. At 10 AoA, the numerical and experimental values for lift coefficient are similar and after that angle, the deviation approximated around 11.5 percent. At 20 m/s, the deviation from 0 to 14 AoA approximated around 22.2 percent and 4.9 percent after the AoA. At 30 m/s, the deviation from 0 to 16 AoA approximated around 22.6 percent and 0.7 percent after that angle. This shows that as the velocity increase, the deviation is decreased at higher angle of attack.

In the second case, at 10 m/s the deviation is found to be 18.9 percent from 0 to 14 AoA and 6 percent after that angle. At 20 m/s, for 0 AoA, the difference between experiment and numerical is 14.7 percent. From 2 to 18 AoA, the deviation is 13.2 percent and the difference at 20 AoA is 1.8 percent.. At 30 m/s, from 0 to 18 AoA, the deviation approximated around 18 percent and the difference between experiments and numerical at 20 AoA is also 1.8 percent.

In the third case, at 10 m/s the deviation is found to be 4.1 percent from 0 to 2 AoA, 4.7 percent from 4 to 6 AoA, 2.2 percent from 8 to 12 AoA, 12.3 percent from 14 to 16 and 8.6 percent from 18 to 20 AoA. At 20 m/s, the deviation approximated around 18 percent from 0 to 18 AoA and the difference between experiments and numerical for 20 AoA is 8.9 percent. At 30 m/s, from 0 to 16 AoA, the deviation approximated around 24.7 percent and 15.2 percent from 18 to 20 AoA. For this case, the lift coefficient is vice versa from case 1 and 2 where as the velocities increase the deviation is increase at higher angle of attack. However, the percent deviation at lower angle of attack is smaller compared with previous both cases.

4.4.2 Drag Coefficient

For drag coefficient, in each case, as the velocity increase the drag coefficient approximated shown in the analyses elaborates for each case as below.

For the first case at 10 m/s, the deviation approximated around 61.5 percent from 0 to 16 AoA. From 18 to 20 AoA, the deviation approximated around 16.9 percent. At 20 m/s, the deviation from 0 to 16 AoA approximated around 45 percent and 25.3 percent from 18 to 20 AoA. At 30 m/s, the deviation from 0 to 16 AoA approximated around 17 percent and 16.7 percent from 18 to 20 AoA.

In the second case, at 10 m/s the difference for experimental and numerical result at 0 AoA is 32.3 percent and the deviation approximated around 27.8 percent from 2 to 20 AoA. At 20 m/s, from 0 to 14 AoA, the deviation approximated around 8.5 percent and 13.2 percent from 16 to 20 AoA. At 30 m/s, from 0 to 14 AoA, the deviations approximated around 10.7 percent and the difference between experiments and numerical at 16 and 18 AoA are 9.5 and 5.6 percent respectively. At 20 AoA, the difference is 23.9 percent.

In the third case, at 10 m/s the deviation is found to be 57.4 percent from 0 to 16 AoA and 8.4 percent from 18 to 20 AoA. At 20 m/s, the deviation approximated around 30.2 percent from 0 to 12 AoA, 7 percent from 14 to 16 AoA. At 18 and 20 AoA, the difference between experiment and numerical founded to be 21 and 17.2 percent respectively. At 30 m/s, from 0 to 12 AoA, the deviation approximated around 21.2 percent and 6.1 percent from 14 to 16 AoA. At 18 and 20 AoA, the difference between experiment and numerical approximated around 6 and 94 percent respectively.

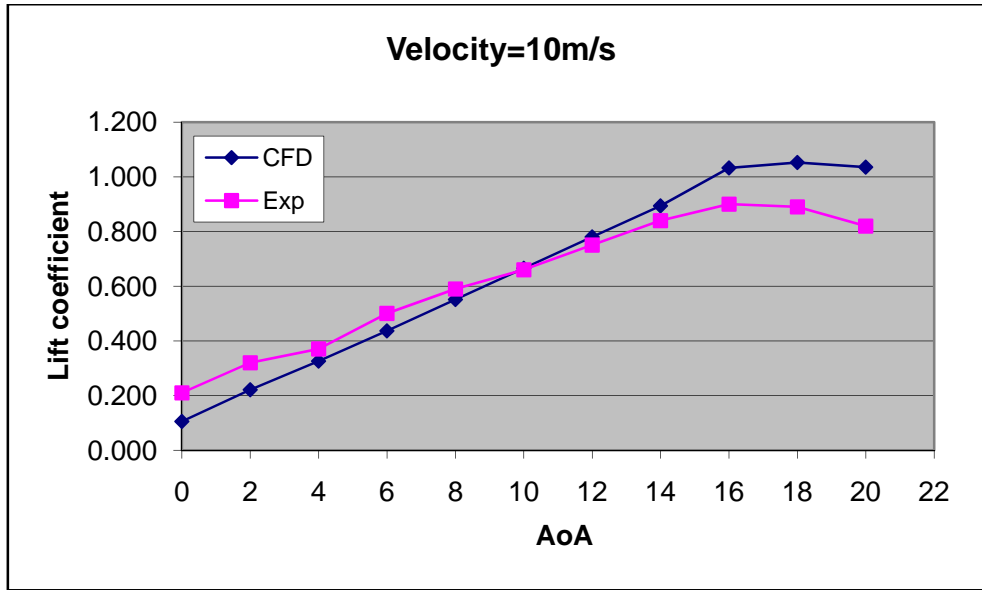


Figure 4.22: Comparison of numerical and experimental results of lift coefficient versus angle of attack for single airfoil

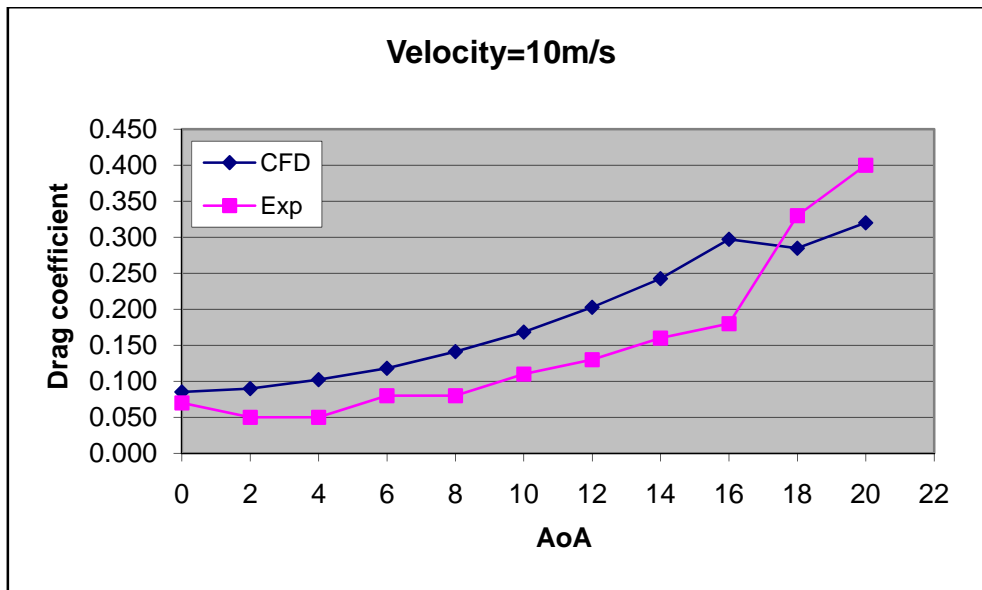


Figure 4.23: Comparison of numerical and experimental results of drag coefficient versus angle of attack for single airfoil

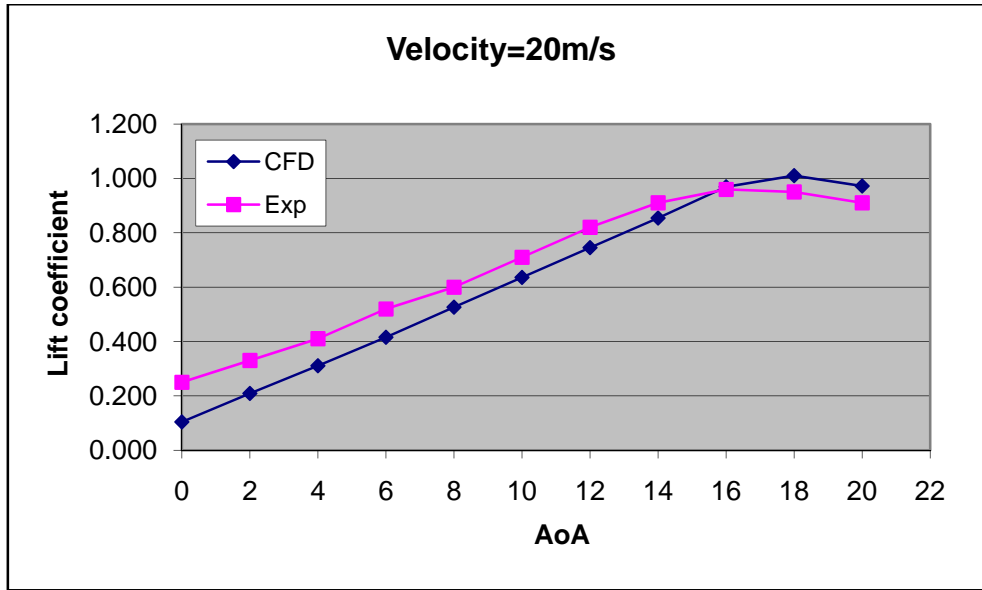


Figure 4.24: Comparison of numerical and experimental results of lift coefficient versus angle of attack for single airfoil

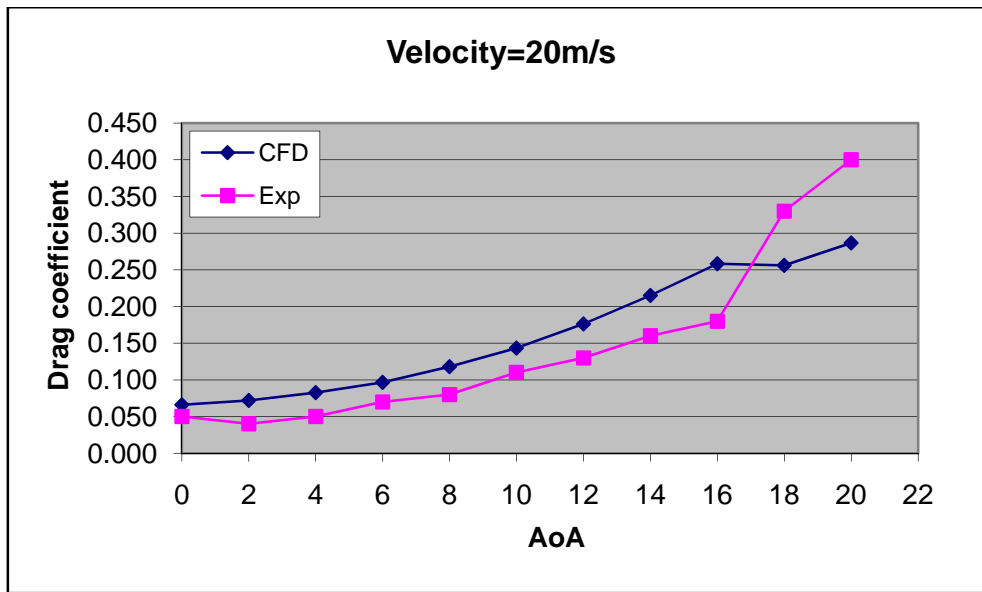


Figure 4.25: Comparison of numerical and experimental results of drag coefficient versus angle of attack for single airfoil

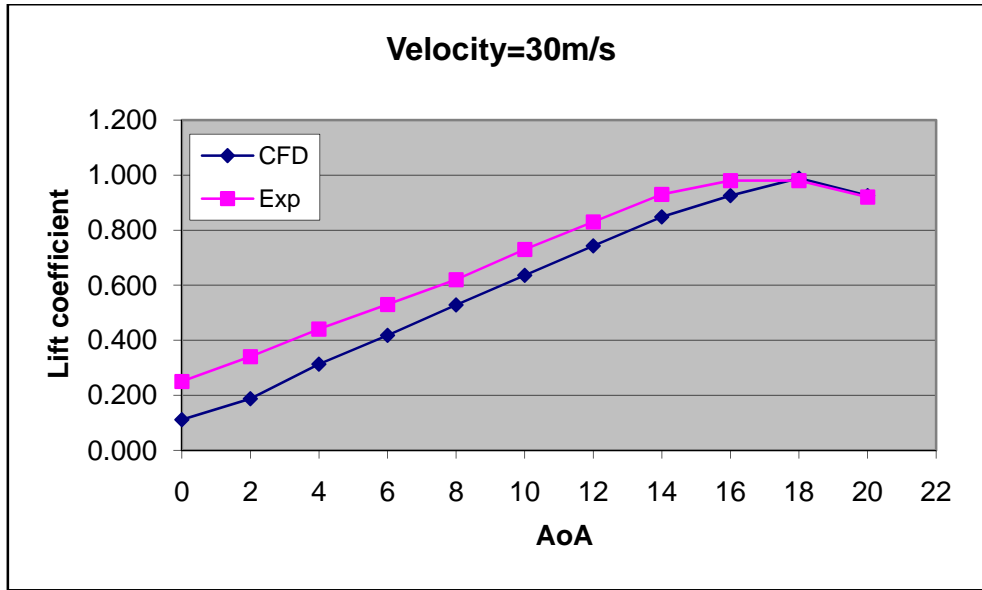


Figure 4.26: Comparison of numerical and experimental results of lift coefficient versus angle of attack for single airfoil

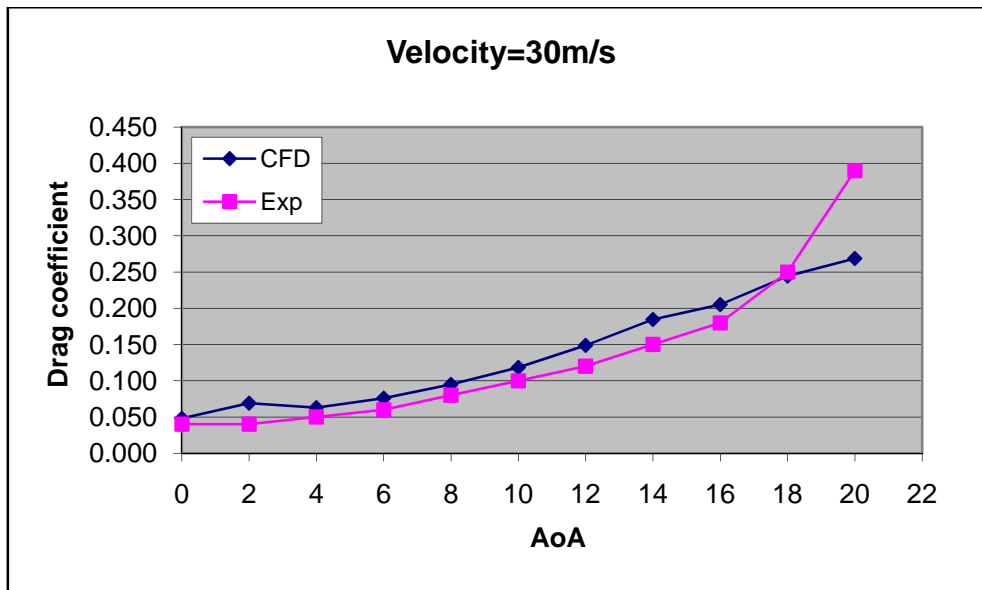


Figure 4.27: Comparison of numerical and experimental results of drag coefficient versus angle of attack for single airfoil

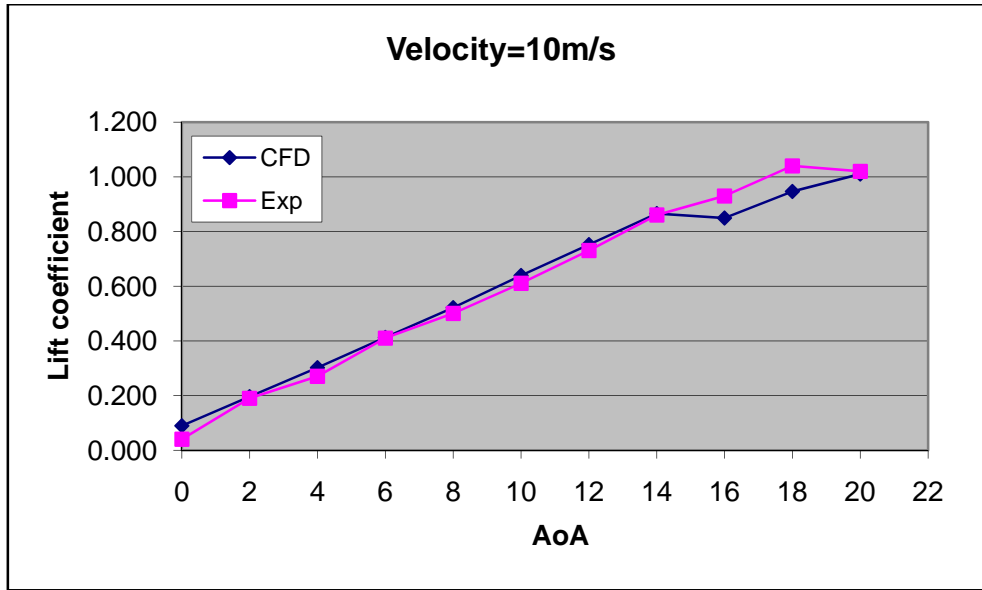


Figure 4.28: Comparison of numerical and experimental results of lift coefficient versus angle of attack for two airfoil at 0.13 m separation distance

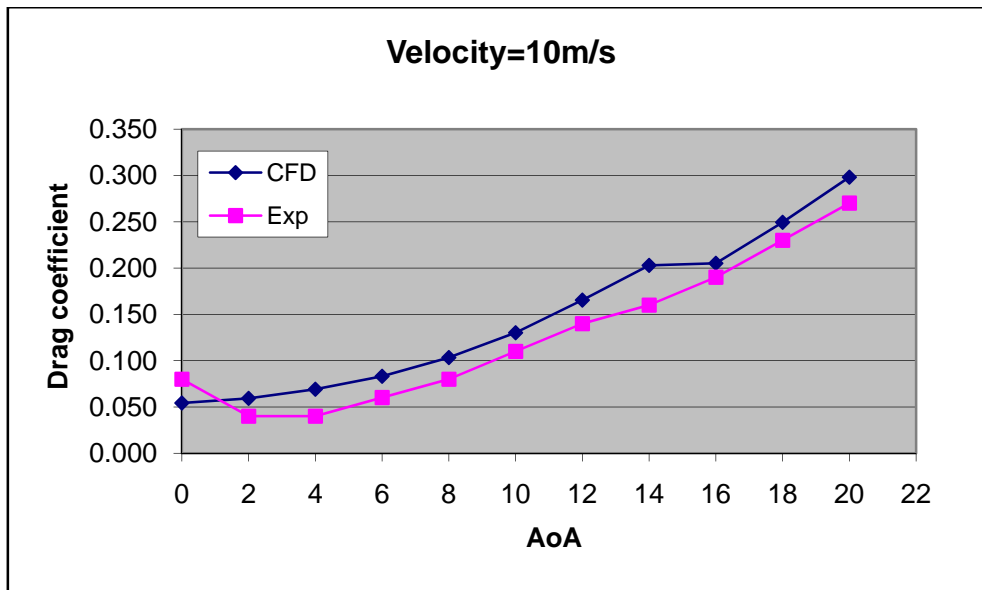


Figure 4.29: Comparison of numerical and experimental results of drag coefficient versus angle of attack for two airfoil at 0.13 m separation distance

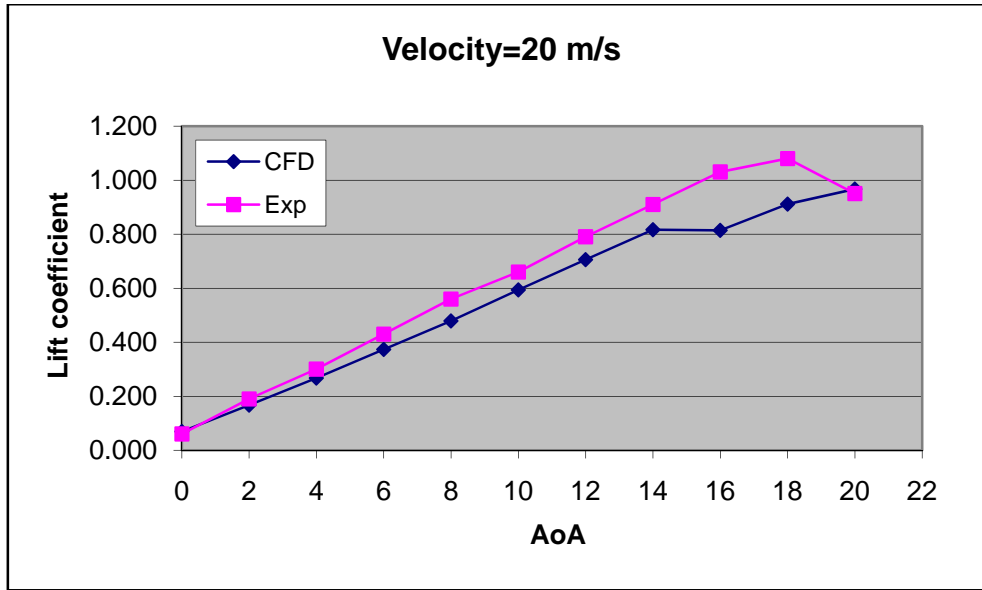


Figure 4.30: Comparison of numerical and experimental results of lift coefficient versus angle of attack for two airfoil at 0.13 m separation distance

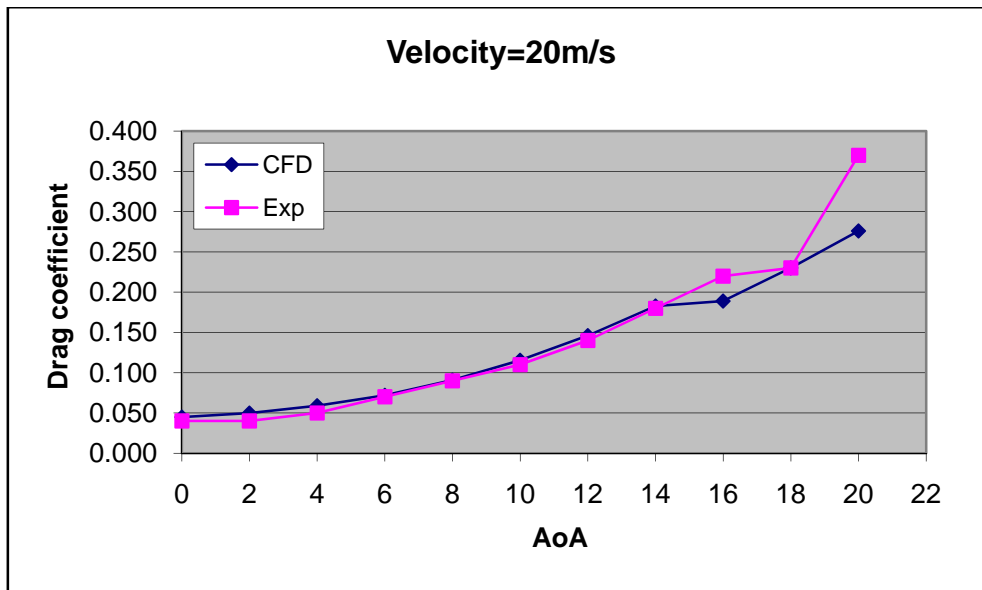


Figure 4.31: Comparison of numerical and experimental results of drag coefficient versus angle of attack for two airfoil at 0.13 m separation distance

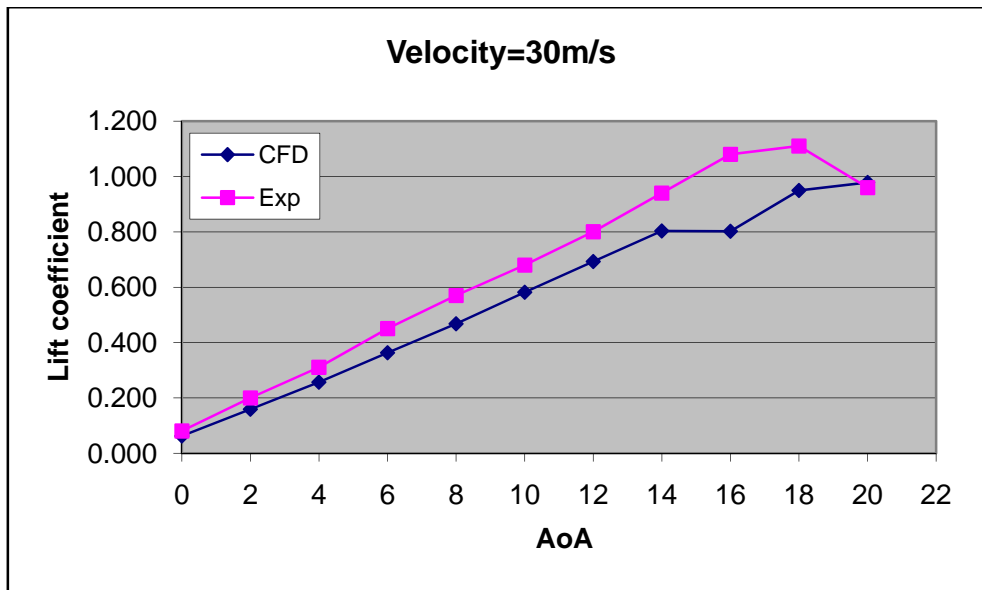


Figure 4.32: Comparison of numerical and experimental results of lift coefficient versus angle of attack for two airfoil at 0.13 m separation distance

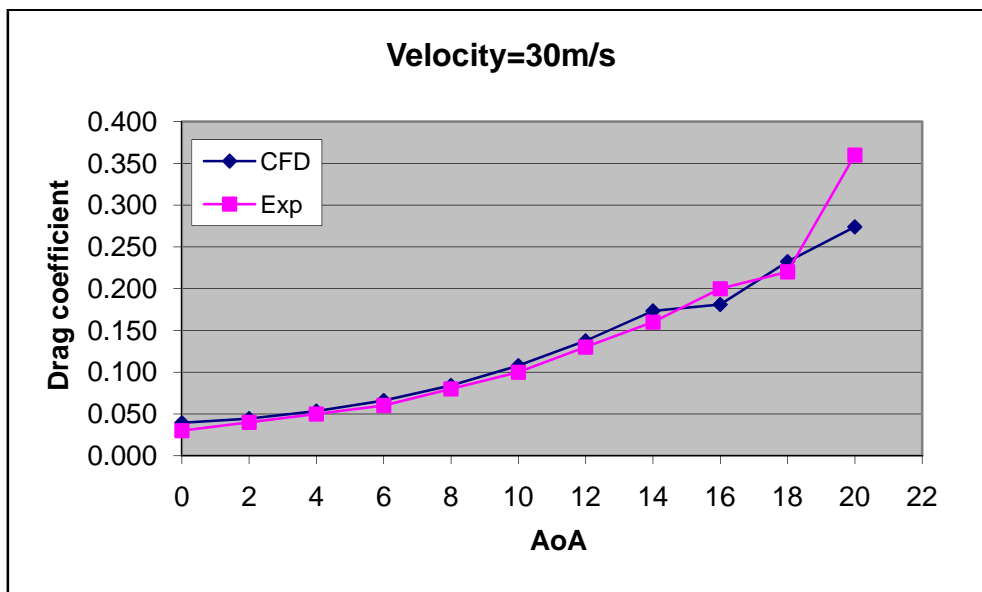


Figure 4.33: Comparison of numerical and experimental results of drag coefficient versus angle of attack for two airfoil at 0.13 m separation distance

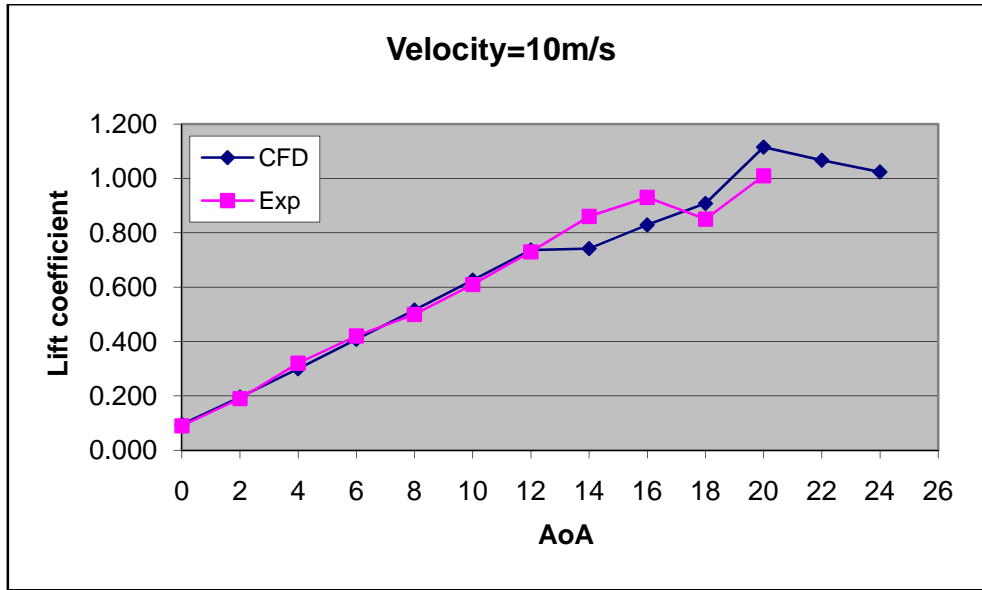


Figure 4.34: Comparison of numerical and experimental results of lift coefficient versus angle of attack for two airfoil at 0.26 m separation distance

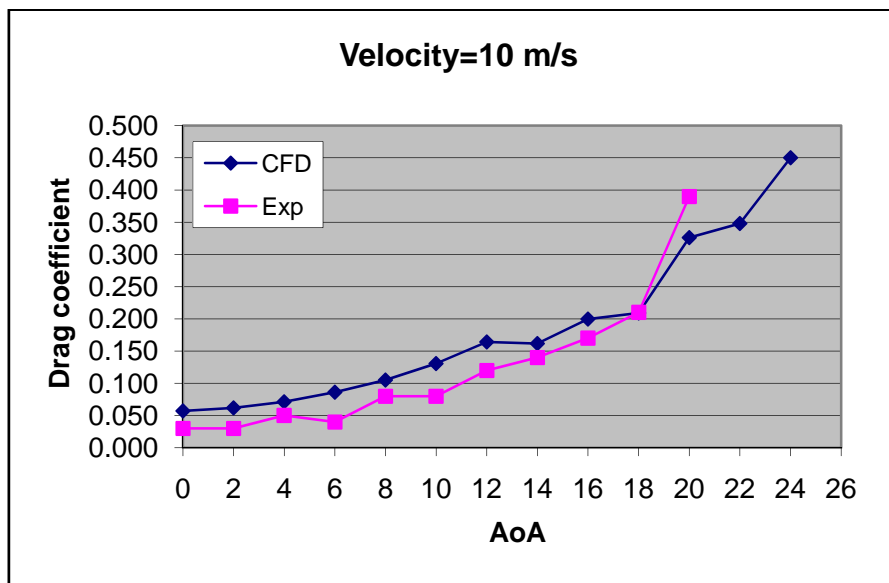


Figure 4.35: Comparison of numerical and experimental results of drag coefficient versus angle of attack for two airfoil at 0.26 m separation distance

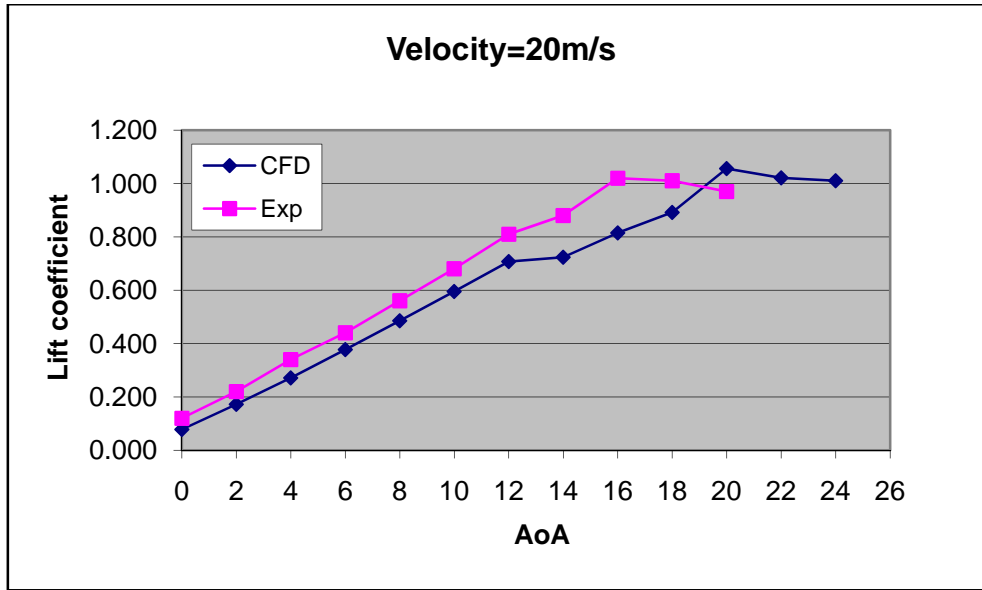


Figure 4.36: Comparison of numerical and experimental results of lift coefficient versus angle of attack for two airfoil at 0.26 m separation distance

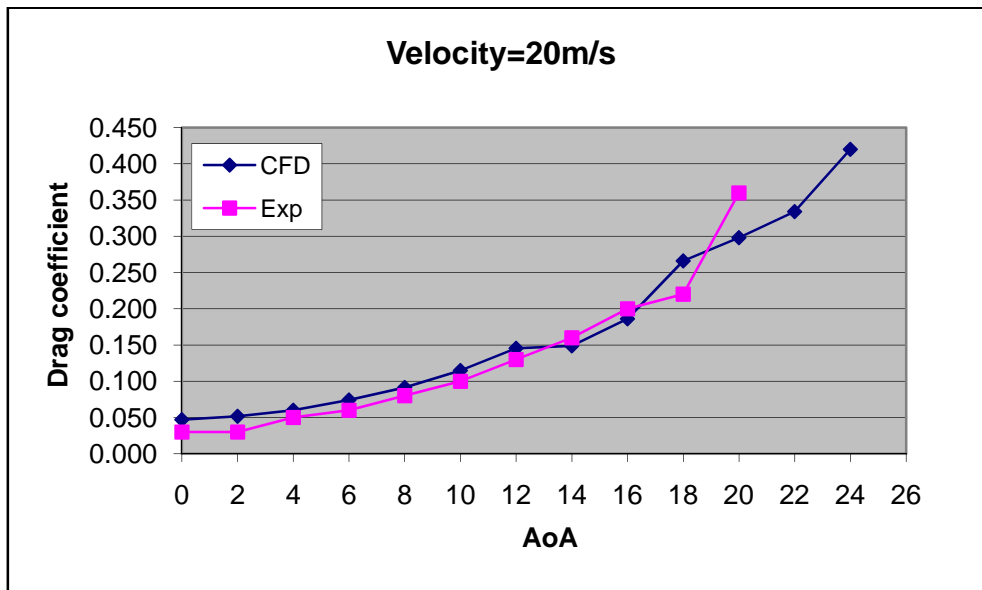


Figure 4.37: Comparison of numerical and experimental results of drag coefficient versus angle of attack for two airfoil at 0.26 m separation distance

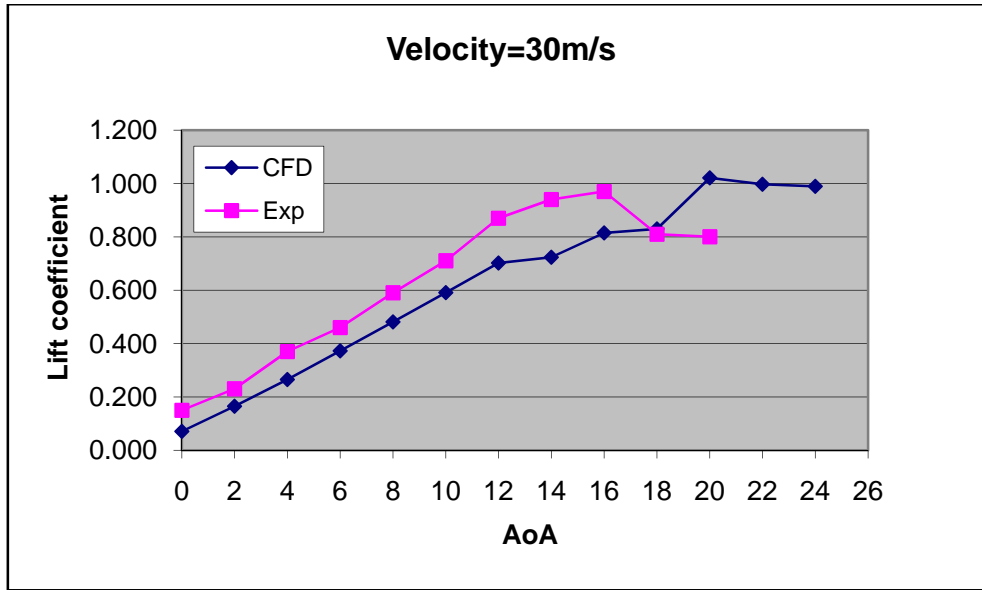


Figure 4.38: Comparison of numerical and experimental results of lift coefficient versus angle of attack for two airfoil at 0.26 m separation distance

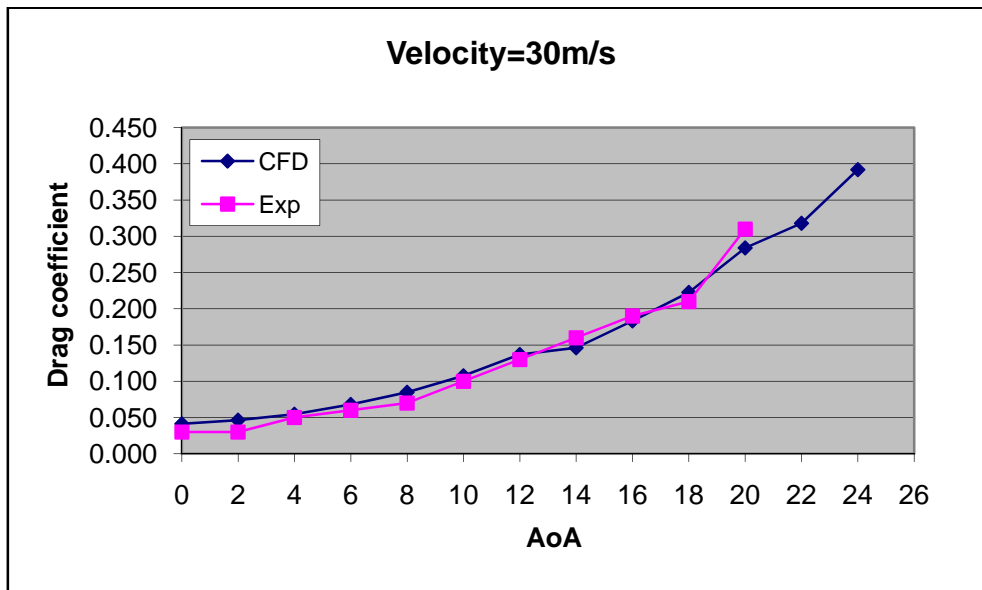


Figure 4.39: Comparison of numerical and experimental results of drag coefficient versus angle of attack for two airfoil at 0.26 m separation distance

CHAPTER 5

CONCLUSIONS AND RECOMMENDATIONS

5.1 Conclusions

The analysis of lift coefficient for the three cases shows that as the velocity increase for the first and second case comparison, the percent difference increasing from 7.8 percent to 14 percent and same goes for the comparison between the first and third case. However, for the second and third case comparison, it was founded that the percent difference is decreasing at 20 m/s around 2.8 percent from 6.2 percent and increasing at 30 m/s to 4.1 percent. The analysis also shows that as the angle of attack increase for the first and second case comparison and first and third case comparison shows that the percent difference is decreasing. However, for the second and third case comparison, the percent difference does not have trend but the value difference is less than 13 percent. For drag coefficient analysis, it also shows that the same trend as lift coefficient where as the velocity increase, the percent difference is decrease for the first case comparison with second and third case. For the second and third case comparison, the percent difference is decreasing from 3.1 percent to 2.8 percent at 20 m/s and increase at 30 m/s to 3.0 percent. The angle of attack also shows the same trend as lift coefficient. From the analysis of percent differentiation, it is clearly shows that the difference between the second and the third case is due to the wake effects that are significant in the second case due to smaller separation distance.

5.2 Recommendations

In order to improve the accuracy of the result, smaller mesh size is recommended to be used for modelling. Besides, the type of mesh elements used also can be changed to get better mesh. However, to confirm this, grid dependency test is recommend to be done. For the simulation settings, changing the convergence criterion from 0.001 to smaller values increase the accuracy of the result obtain. In addition, the turbulence model related to each velocity and discretization for higher angle of attack should be study further as it needs improvement. Lastly, for the analysis purposes, it is recommended simulating all the cases with more set of velocity values in order to obtain a better trend for the lift and drag coefficients. Number of cases simulate also should be increase to get better analysis of wake effects.

REFERENCES

- [1] Tony, M. *Introduction To Flight: A resource supporting the third edition of The BP Technology Challenge File.*(2nd ed.,pp. 10-17). The Royal Society of New Zealand.
- [2] H.Hu,Z.Yang & H.Igarashi (2007). *Aerodynamics Hysterisis of a low Reynolds-Number Airfoil (Journal of Aircraft)*
- [3] Tom, E. (2006). Effects of Wake Vortices on Commercial Aircraft. AME 48491: Undergraduate Research Department of Aerospace and Mechanical Engineering University of Notre Dame
- [4] Khairul N.I. (2008). Study on the Effects of the Wake of an Aircraft on a Following Aircraft. Final Year Project Report of University Technology Petronas.

LIST OF APPENDIX

APPENDIX I	Project Gantt Chart
APPENDIX II	Gambit Modeling
APPENDIX III	Lift and Drag Coefficient versus Angle of Attack

APPENDIX I

PROJECT GANTT CHART

First semester (July 2008)															
No	Tasks	1	2	3	4	5	6	7	8	9	10	11	12	13	14
1	Literature research- gathering data on wake formation and numerical approach	█	█	█	█							█			
2	Wing selection and turbulence modeling					█	█	█				█			
3	Modeling								█	█	█	█			
4	Simulation scheming											█	█	█	█
Second semester (January 2009)															
1	Simulations	█	█	█	█	█	█	█	█	█	█	█			
2	Data analyzing											█	█	█	█
<div style="display: flex; align-items: center; justify-content: center;"> <div style="width: 40%; height: 15px; background-color: #cccccc; margin-right: 10px;"></div> mid-semester break </div>															

APPENDIX II

GAMBIT MODELING STEPS

NACA 2412 Coordinates

18 2

0 0 0

0.001625 0.002795 0

0.00325 0.003887 0

0.0065 0.005369 0

0.00975 0.006448 0

0.013 0.007319 0

0.0195 0.008593 0

0.026 0.009438 0

0.0325 0.009971 0

0.039 0.010244 0

0.052 0.01014 0

0.065 0.009412 0

0.078 0.008268 0

0.091 0.006734 0

0.104 0.004875 0

0.117 0.002704 0

0.1235 0.001482 0

0.13 0 0

0.13 0 0

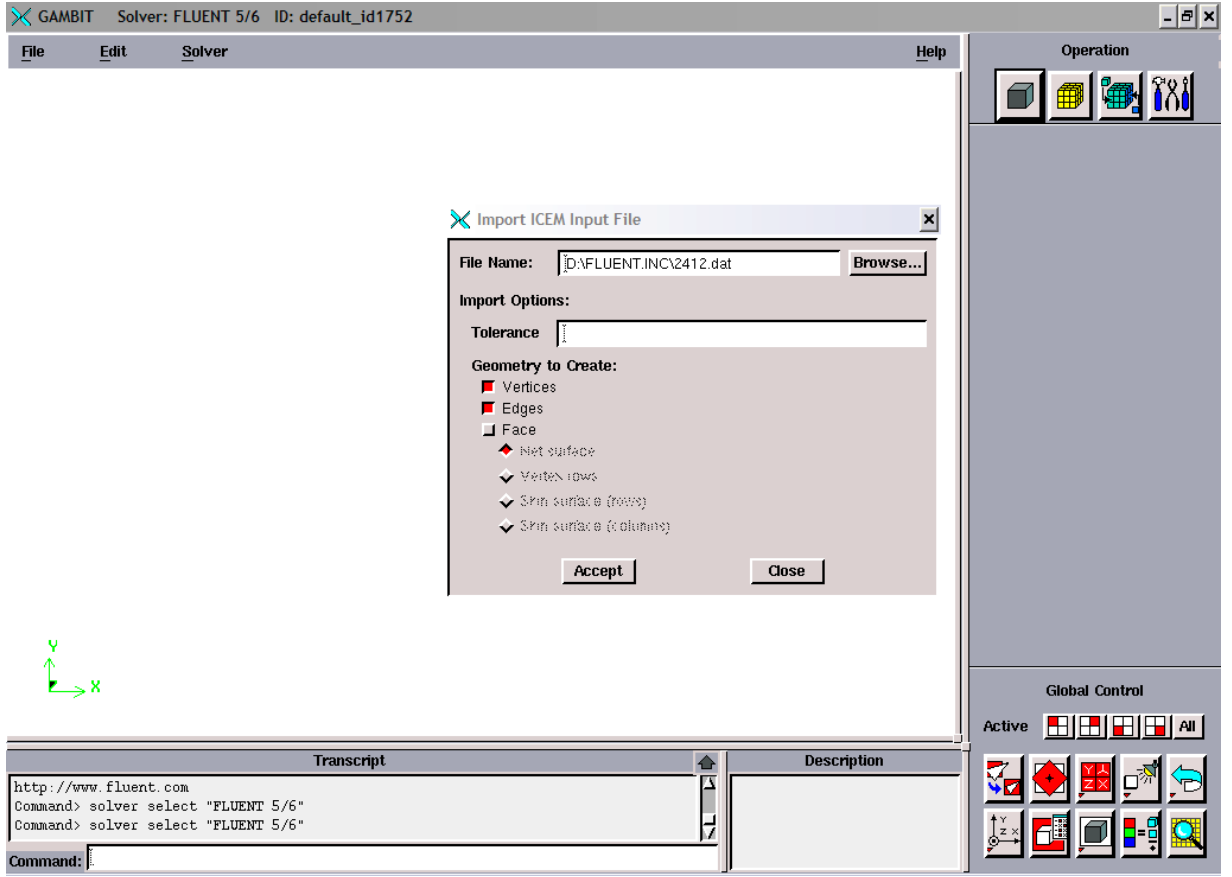
0.1235 -0.000624 0

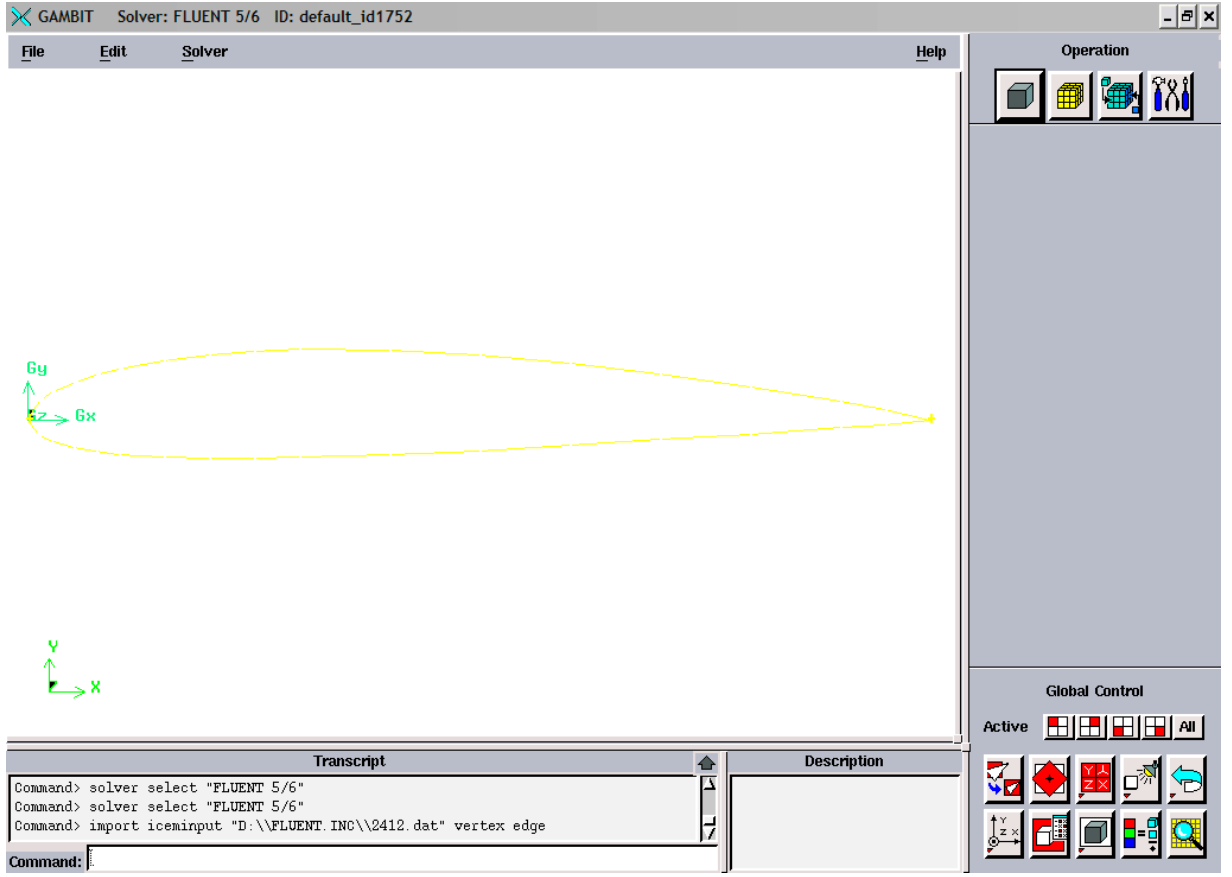
0.117 -0.001066 0

0.104 -0.00195 0


0.091 -0.002782 0

0.078 -0.003588 0
0.065 -0.004342 0
0.052 -0.00494 0
0.039 -0.005356 0
0.0325 -0.005486 0
0.026 -0.005499 0
0.0195 -0.00533 0
0.013 -0.004875 0
0.00975 -0.004498 0
0.0065 -0.003913 0
0.00325 -0.002951 0
0.001625 -0.002145 0
0 0 0






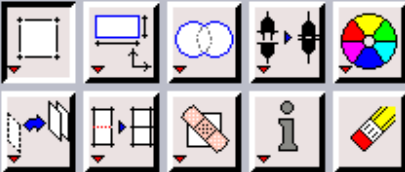
Operation





Geometry



Face



Create Face From Wireframe

Edges  

Type: Real Virtual





Create planar tolerant face


Tolerance:

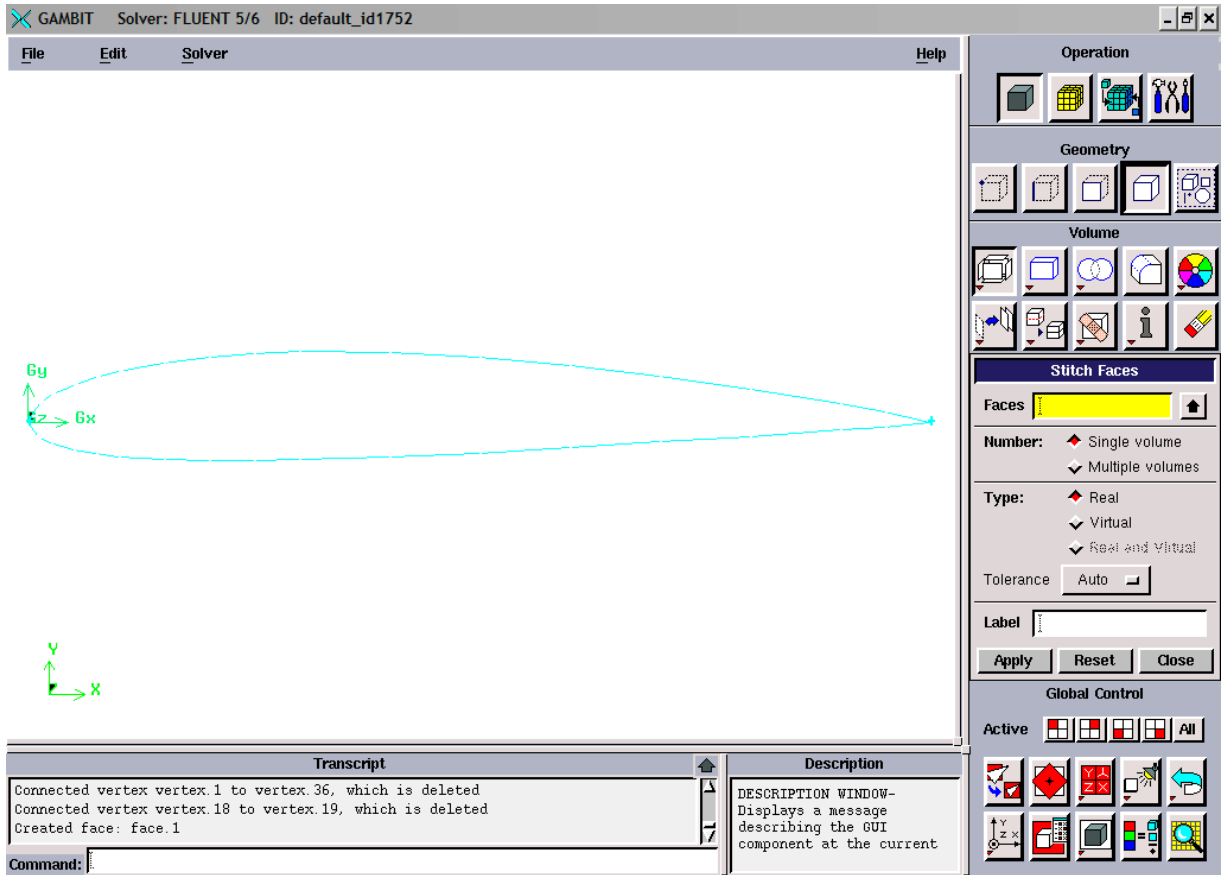
Label

Apply **Reset** **Close**

Global Control

Active     **All**





Vector Definition

Active Coordinate System Vector

Start: (0, 0, 0)

End: (0, 0, 1)

Magnitude

Method:

Coordinate Sys.

Direction:

X Positive Negative

Y Positive Negative

Z Positive Negative

Geometry

Volume

Sweep Faces

Faces

Path: Edge Vector

(0, 0, 0) -> (0, 0, 1)

With mesh

Type: Rigid Perpendicular


Option: Draft Twist

Angle


Type: Extended Round Mined

Label

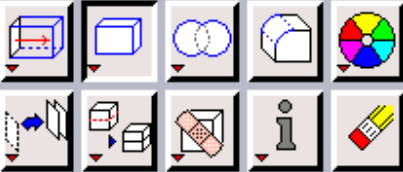
Operation



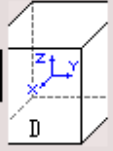
Geometry



Volume




Create Real Brick

Width(X) 

Depth(Y)

Height(Z)


Coordinate Sys. 

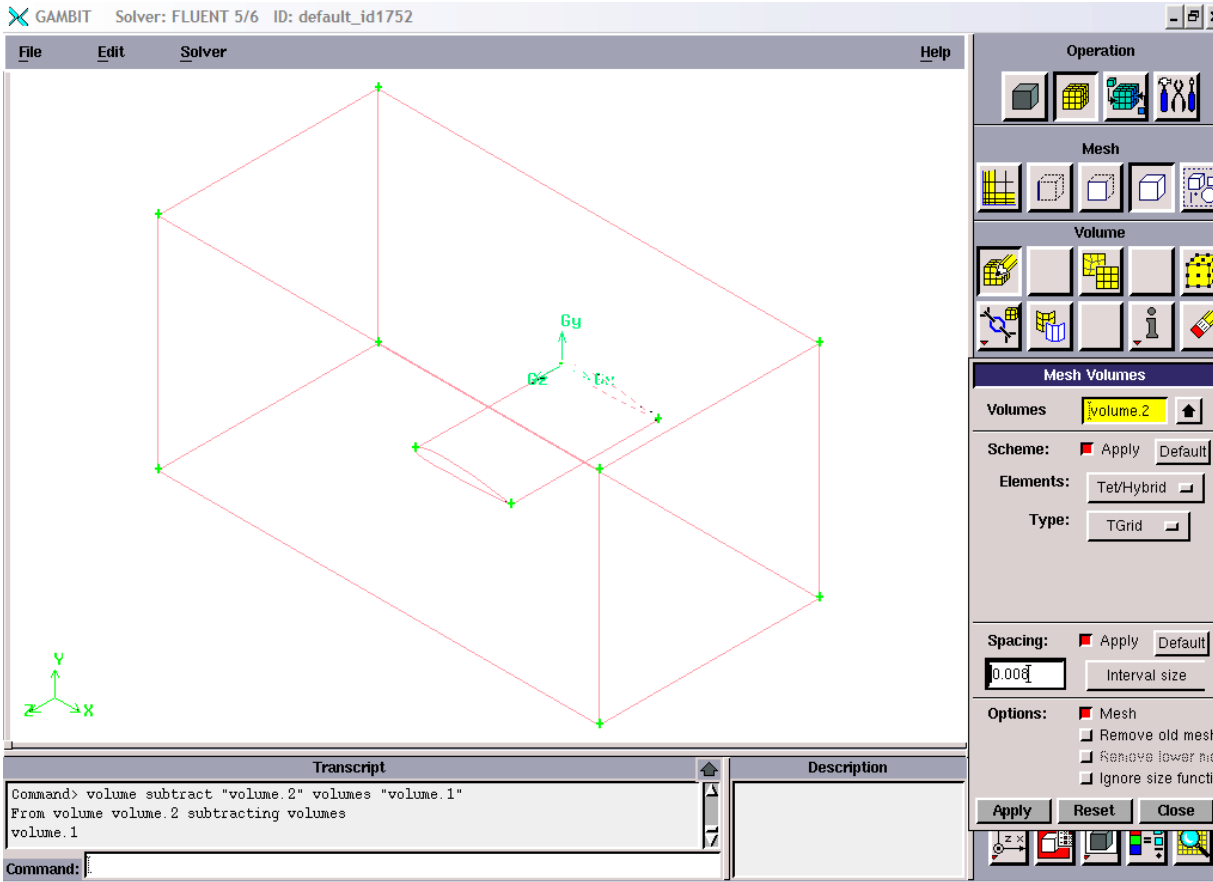
Direction

Label

Global Control

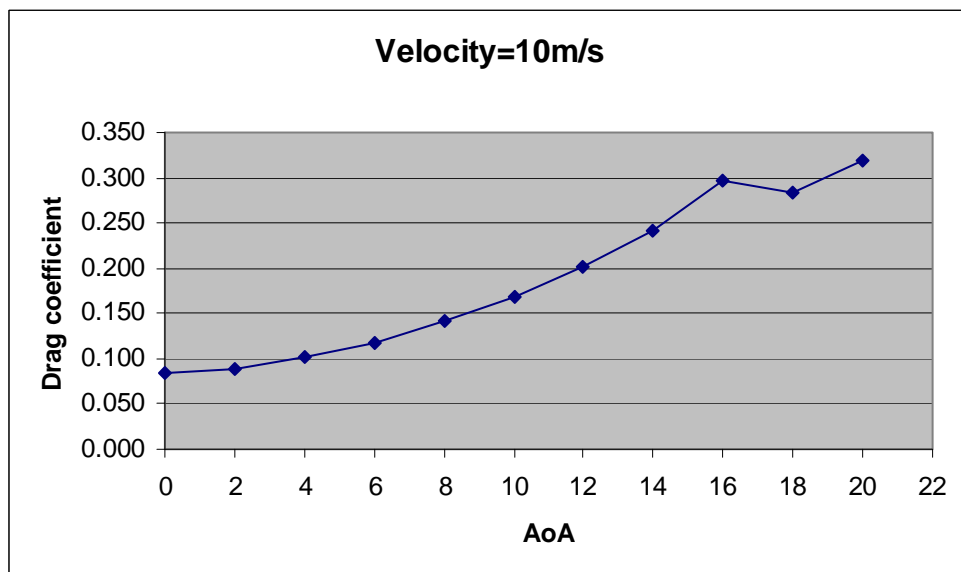
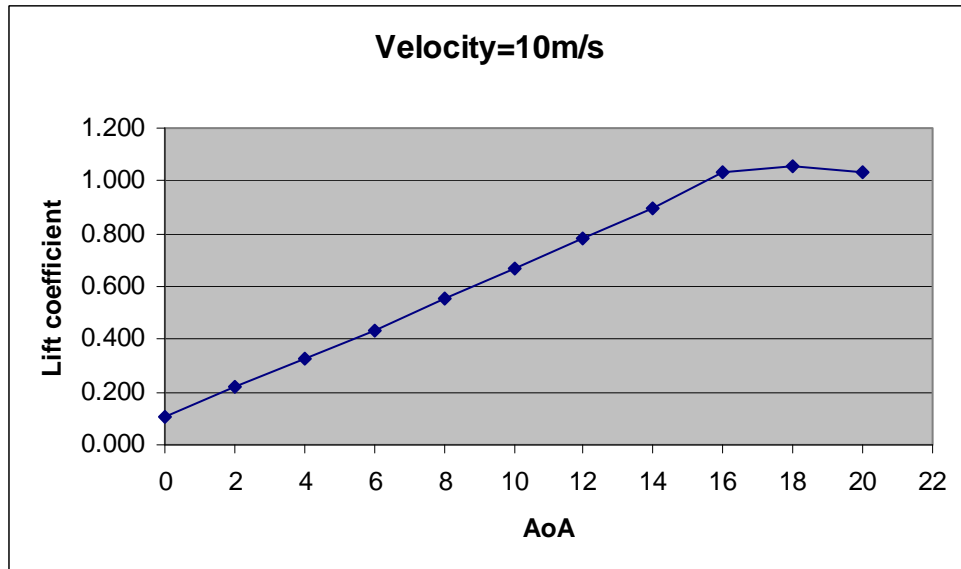
Active All

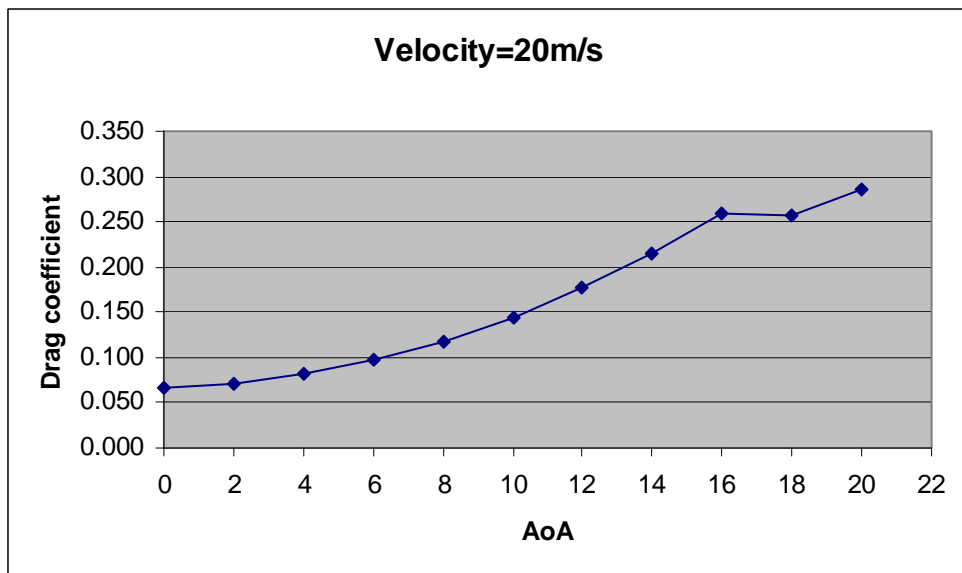
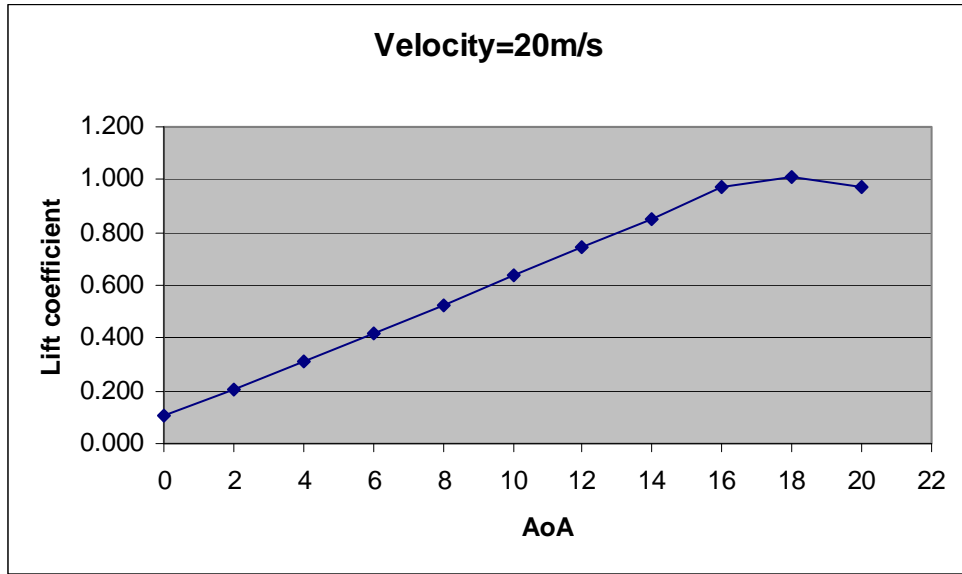


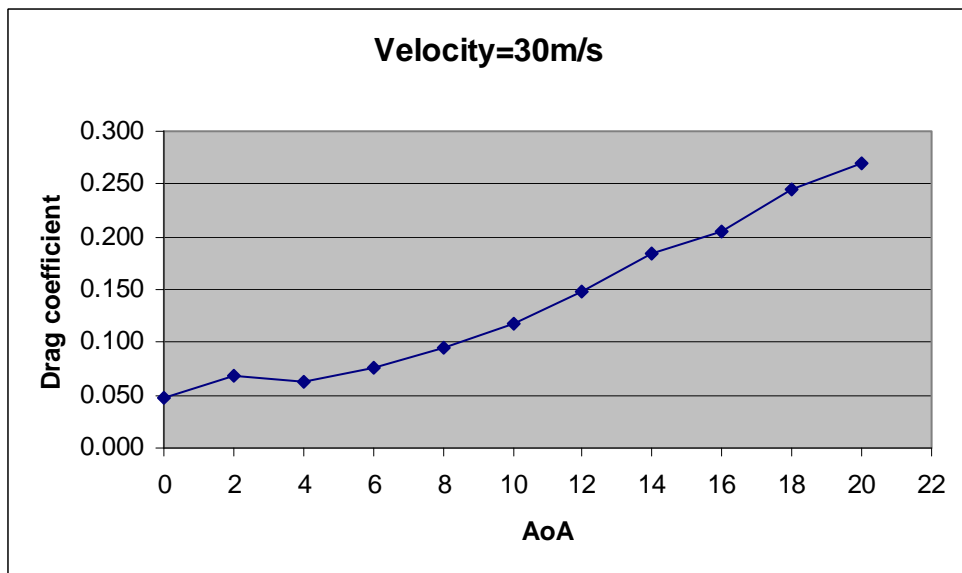
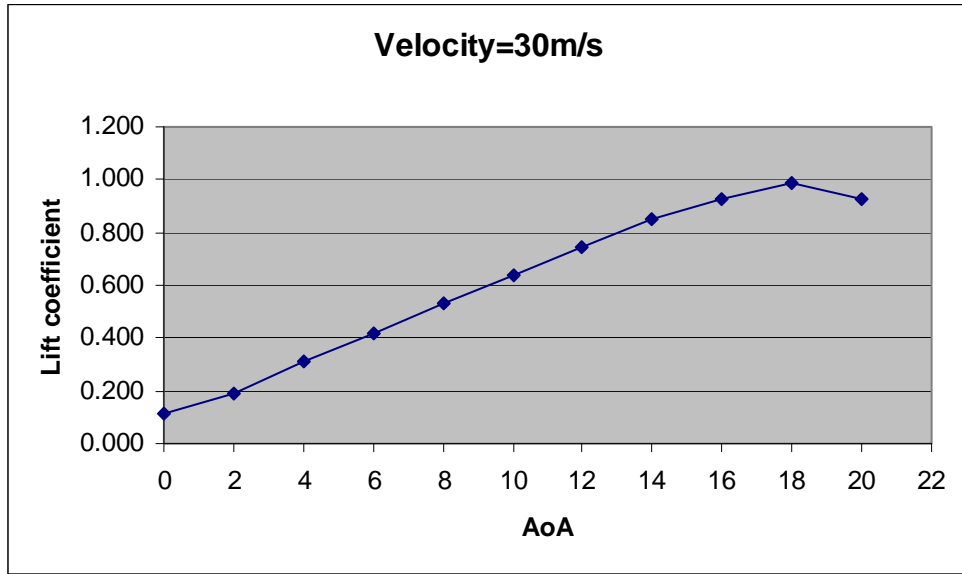


APPENDIX III

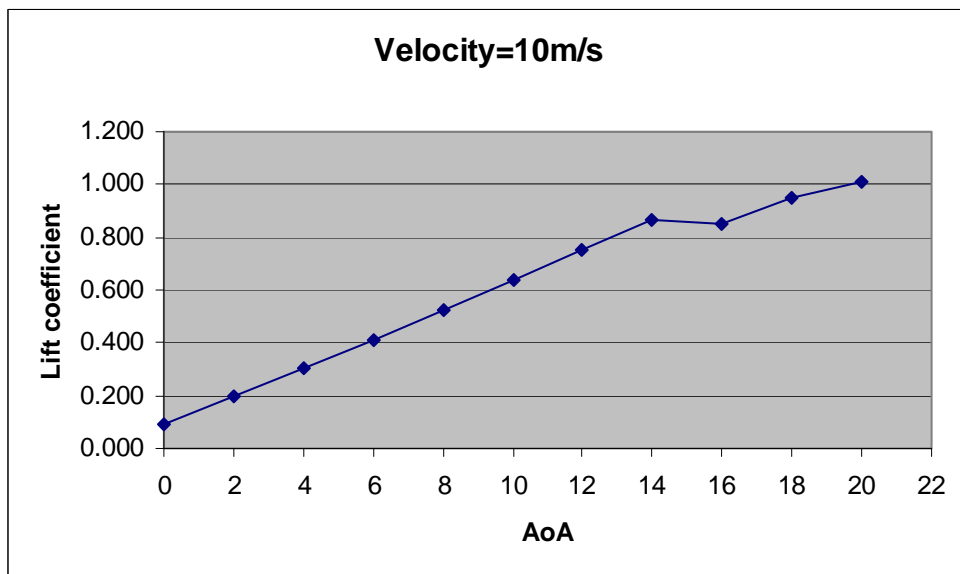
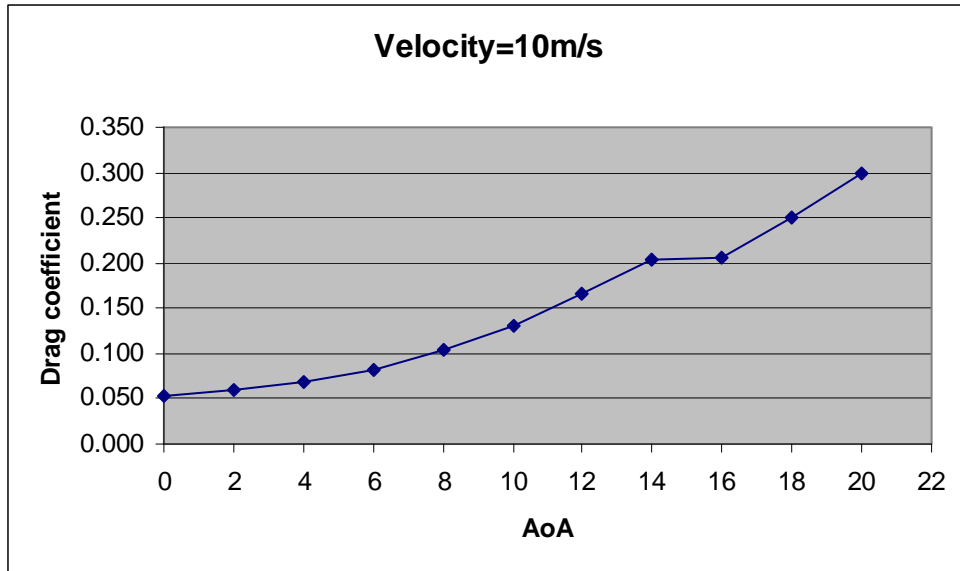
Single airfoil

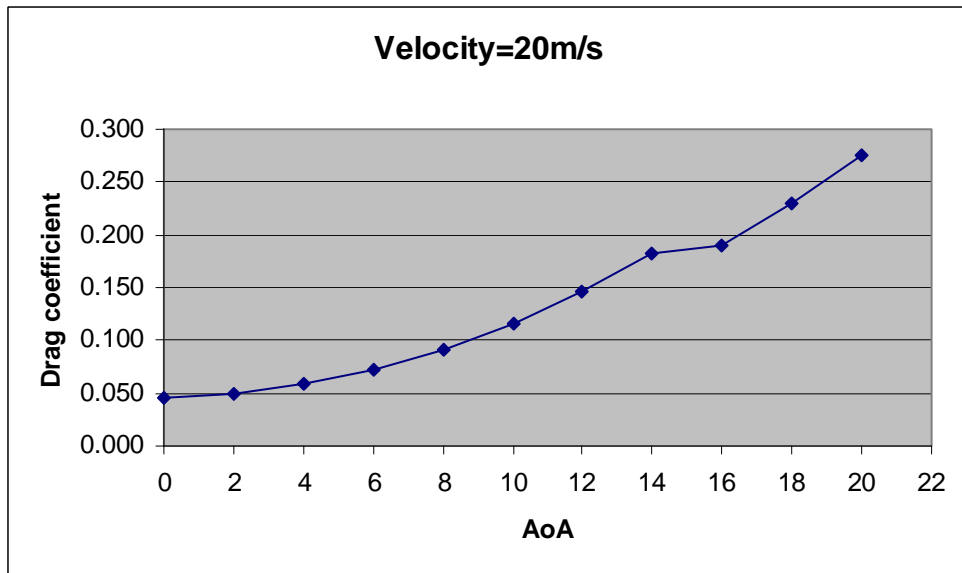
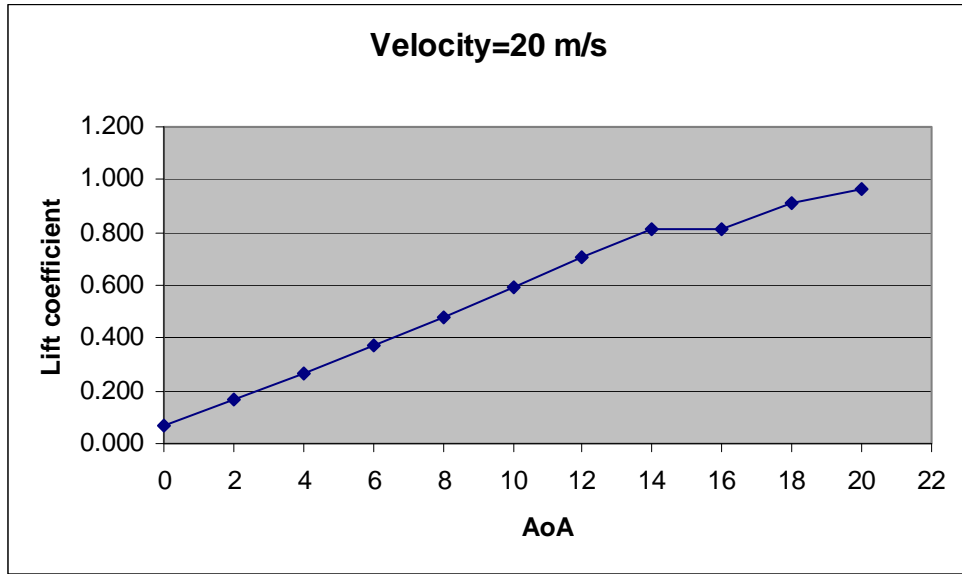


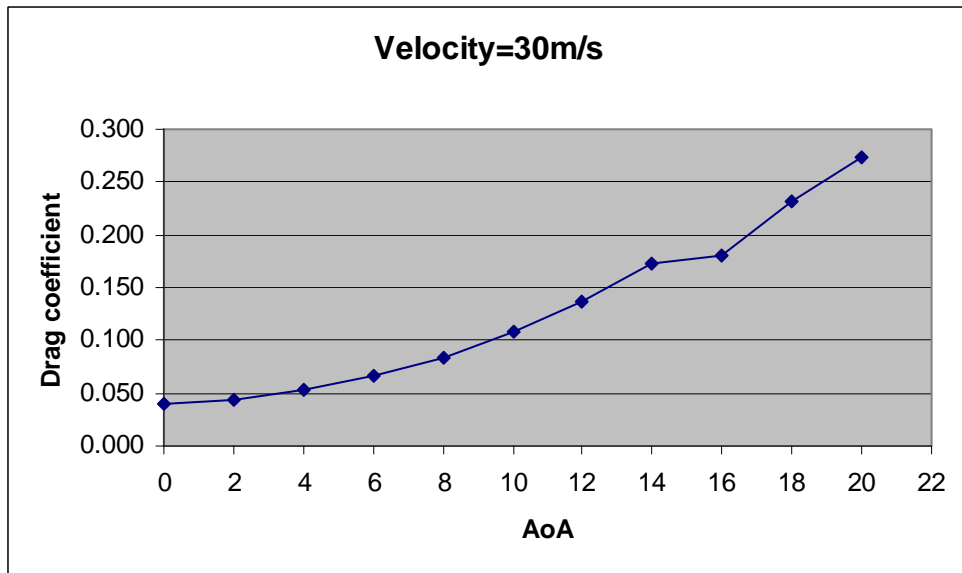
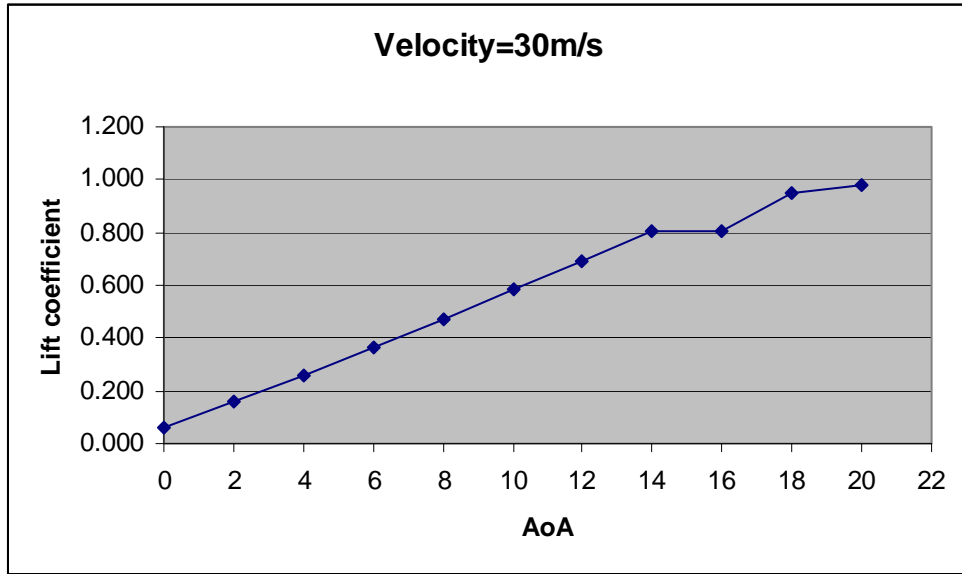




Two airfoils separated at 0.13 m separation distance







Two airfoils separated at 0.26 m separation distance

